Universidade de Aveiro
Ano 2012

Departamento de Ambiente e Ordenamento (DAO)

INTI ERNESTO LUNA AVILÉS

Processamento de imagens de veículos aéreos não tripulados para estudos da vegetação

Processing Images from Unmanned Aerial Vehicles for Vegetation Studies

Universidade de Aveiro
Ano 2012

Departamento de Ambiente e Ordenamento (DAO)

INTI ERNESTO LUNA AVILÉS

Processamento de imagens de veículos aéreos não tripulados para estudos da vegetação

Dissertação apresentada à Universidade de Aveiro para cumprimento dos requisitos necessários à obtenção do grau de Mestre em Estudos Ambientais (JEMES), realizada sob a orientação científica do Doutor Jan Jacob Keizer, Professor Investigador do Departamento de Ambiente e Ordenamento (DAO) da Universidade de Aveiro e a co-supervisao do Doutor Agustín Lobo Aleú, Professor da Universidade Autonóma de Barcelona e Investigador do Institut de Ciencies de la Terra "Jaume Almera" (CSIC).

Processing Images from Unmanned Aerial Vehicles for Vegetation Studies

Thesis submitted to the University of Aveiro to fulfill the requirements for the degree of Master of Environmental Studies (JEMES), held under the scientific guidance of Dr. Jan Jacob Keizer, Research Professor, Department of Environment and Planning (DAO) of the University of Aveiro and co-supervision of Dr. Agustin Lobo Aleu , Professor at the Autonomous University of Barcelona and researcher at the Institut de Ciencies de la Terra "Jaume Almera" (CSIC).

O Júri Presidente	Professora Doutora Ana Isabel Couto Neto da Silva Miranda. Professora Associada com agregaçao, Departamento de Ambiente e Ordenamento- Universidade de Aveiro.
Vogal Arguente Principal	Prof. Doutor António J.D. Ferreira. Escola Superior Agraria de Coimbra(ESAC) Instituto Politecnico de Coimbra (IPC)
Vogal Orientador	Doutor Jan Jacob Keizer. Equiparado a Investigador Auxiliar, CESAM- Departamento de Ambiente e Ordenamento da Universidade de Aveiro

Acknowledgment

I appreciate the contributions from many people sharing information and experience. I thank the support from my supervisors and their families, my colleagues, friends and family that were with me during the last two years.

I want to thank the developers of R and QGIS software, their help groups and the open source community.

This work would not exist without the European Union Commission Scholarship Program for the Joint European Master in Environmental Studies.

Palavras-chave mapeamento, vegetação, VANT, agricultura, conservação,

Resumo

O objetivo principal desta tese de mestrado foi avaliar as aplicações ambientais e agrícolas de imagens obtidas com veículos aéreos não-tripulados (VANT) para estudar a vegetação e para avaliar o processamento de imagens envolvido, a fim de obter informação útel e compatível com outro tipo de geo-dados. Imagens dos veículos aéreos não tripulados foram processadas em três diferentes casos de estudo individualmente descritos e analisados com uma estreita relação entre si. (1) mapeamento da cobertura vegetal em um campo de cultivo de cana de açúcar na Nicarágua mostrou a extração operacional e eficaz de geoinformação para a gestão espacial otimizada com fotografia digital simples, mas também colocou em evidência os limites dos sensores sem a banda do infravermelho próximo e a preocupação de chegar a ter uma correção geométrica precisa, em terrenos acidentado. O aspecto particular da correção geométrica, que é fundamental para garantir a ligação confiável entre os produtos derivados das imagens e informação de campo, foi assim abordada nos seguintes dois casos de estudo: (2) correções geométricas de imagens multiespectrais de uma área montanhosa nos Pirenéus espanhóis usando métodos padrão empíricos, e (3) a correção geométrica de imagens usando tecnologia de ajuste de blocos e detecção automática de pontos em imagens do Parque Natural Montseny. A conclusão geral da tese é que as imagens adquirida com VANT são uma solução eficaz para aplicações ambientais e agrícolas de sensoriamento remoto, mas exige um esforço substancial e experiência em processamento de imagens.

Keywords mapping, vegetation, UAV, agriculture, conservation

Abstract

The main goal of this master thesis was to evaluate the environmental and agricultural applications of UAV imagery for studying vegetation and to assess the image processing involved in order to retrieve useful and compatible information with other type of geo-data. Imagery from unmanned aerial vehicles was processed for three different individually described and analyzed study cases with a close relation between each other. (1) Mapping Green Vegetation Cover on a sugarcane crop field in Nicaragua showed the operational and cost-effective retrieval of geoinformation for spatially-optimized management with simple standard digital photography, but also put in evidence the limits of sensors lacking near-infrared bands and the concern of reaching accurate geometric correction with UAV imagery over rugged terrain. The particular aspect of geometric correction, which is critical to ensure reliable link between products derived from the images and field information, was thus addressed in the next two study cases: (2) Geometric Corrections of Multispectral Images of a Mountainous Area in the Spanish Pyrenees using standard empirical methods, and (3) Mosaicking and geometric correction of UAV Imagery using bundle block adjustment and automatic tie point detection technology on images from Montseny Natural Park. The general conclusion of this thesis is that imagery acquired with UAV is a cost-effective solution for environmental and agricultural applications of remote sensing, but requires substantial effort and know-how on image processing.

Table of Contents

List of Figures

List of Tables

List of Abbreviations

AGL. Above Ground Level

AOI. Area of Interest

ASL. Above Sea Level

BBA. Bundle Block Adjustment

DN. Digital Number

GCP. Ground Control Point

GP. Gap Percentage

GVC. Green Vegetation Cover (sometimes used as VC)

IMU. Inertial Movement Unit

OS. Operative System

RPV Remotely Piloted Vehicle

UAV. Unmanned Aerial Vehicle

VANT. Veículos aéreos não-tripulados

VCP. Vegetation Cover Percentage

VI. Vegetation Index or Indices

1.1 Introduction

Vegetation is a key part of the puzzle of understanding climate change, playing a role in carbon, water and energy fluxes while at the same time is being affected by temperature and hydrological changes . Among the consequences of Climate Change, it is likely to have an increment of pest pressure on agriculture, loss of ecosystem integrity that could lead to greater frequency of new emerging diseases (Cramer et al. 2001; Turral et al. 2011).

Therefore, more efforts should be focusing on how to improve the way we manage vegetation, which implies monitoring it in a more regular and viable basis, taking into consideration the cost of acquiring the information. Electromagnetic energy reflected from the Earth surface may be recorded by a variety of remote sensing systems. Traditionally, satellites are used to monitor large areas around the world which is of great help when studying regional phenomena but when the area to be monitored requires a higher revisit rate, or it is on area with high weather variability, then satellites are an expensive alternative and have limitations. One of the new tools for environmental applications and particularly studying vegetation is the use of unmanned aerial vehicles which offers some advantages over conventional remote sensing platforms, such as the operative costs, more spatial and temporal resolution required to study highly variable aspects of diversity and structure of vegetation(Burdekin et al. 2002).

Despite all this advantages many limitations still exist regarding the processing and retrieving useful information from images acquired with UAVs, considering the cost of the sensor, operational capabilities, different resolutions (spatial, temporal, spectral and radiometric) and the present infrastructure for storage and analysis of such information.

1.2 Background

Unmanned Aerial Vehicles (UAVs) have been referred to as RPVs (remotely piloted vehicle), drones or robot planes. These vehicles were tested during World War I, but not used in combat by the United States during that war. Germany's use of the simple yet deadly V-1 "flying bomb" during World War II, laid the groundwork for post-war UAV programs in the United States. However, it was not until the Vietnam War that UAVs such as the AQM-34 Firebee were used in a surveillance and target acquisition role and just recently it was modified to deliver payloads and flew its first flight test as an armed UAV on December 20, 2002 (Morris, Jefferson 2003). As a proof of the increment of use and importance of these vehicles just in the military sector in the USA, the department of defense had increased the inventory of UAVs more than 40-fold from 2002 to 2010 (Johnson and Schrage 2004).

UAV are classified based on several characteristic including endurance, weight, altitude, dimensions, landing capabilities among others. One simple classification base on weight is presented in **table 1.1**. Most of the UAV used for environmental and agricultural applications are micro and light-weight including the ones use in the present study.

Table 1.1. Classification of UAV based on weight[1].

Classification	Weight (kg)
Super Heavy	>2000
Heavy	200-2000
Medium	50-200
Light	5-50
Micro	<5

1Table taken from Arjomandi (2007)

These vehicles have been used to retrieve biological information for conservation (Lobo Aleu 2009), to study riparian forest in the Mediterranean (Dunford et al. 2009), to study rangeland environments (Laliberte et al. 2011),to measure greenhouse gases concentration in the atmosphere (Khan et al. 2012), and radiation in post-disaster environment of Fukushima nuclear reactor explosion(Towler et al. 2012), among many others environmental applications that are under current extensive research.

Although the same principles and techniques are used for satellites, conventional aerial imagery and UAV. There are some important difference related with the nature of the images and the quality of the sensors that are in general of lower profile in the case of UAVs. In addition, Image Processing softwares were developed to process images obtained from satellites and professional cameras used in aircraft driven by markets demand. As a consequence, processing much more frames obtained with UAVs covering less area requires others approaches and solutions that are under research by many groups worlwide (Biesemans and Everaerts 2006; Thiele et al. 2008; Grenzdörffer et al. 2008; Niethammer et al. 2011; Guo et al. 2012).

1.3 Objective and Thesis Structure

The main goal of this thesis was to evaluate the environmental and agricultural applications of UAV imagery for studying vegetation and to assess the image processing involved in order to retrieve useful and compatible information with other type of geo-data.

In the present work, chapter two covers a case study based on current UAV technology available in Nicaragua and evaluate its potential agronomic applications in a sugarcane crop field. Images acquired with a conventional RGB camera were used to discriminate between green vegetation and ground areas on a flat terrain. As a result, detailed maps with this information are useful for farmers in order to evaluate the quality of the plantation process and for decision making regarding the amount of inputs (water, fertilizer, etc.) to be applied at specific sites in the field.

The third and fourth chapter deal with specific methods to address the problem of geometric correction of this type of imagery over areas with strong relief. Geometric correction is a critical step to provide an operational, effort and cost effective product because ensures the reliable link between the remote sensing data and field information.

In the third chapter, the standard methods of geometric correction of multispectral images was performed and evaluated with images acquired over a mountainous area where there is an Eddy Covariance Tower for studying carbon flux in the Spanish Pyrenees.

In the fourth chapter, a different and more sophisticated approach for geometric correction was performed and evaluated. Images were acquired over the Spanish Natural Park Montseny using a commercial camera (modified to capture NIR light) and the processing for creating orthorectified mosaics was described using a

commercial software which uses bundle block adjustment technology and automatic tie point detection between images.

Joint European Master in Environmental Studies (JEMES)

Chapter 2

Mapping Green Vegetation Cover for Agricultural Applications using Unmanned Aerial Vehicles Visible Imagery

Case Study: Sugarcane field in Nicaragua

by

Inti Luna Avilés

Supervisors:

Jacob Keizer

Agustin Lobo Aleu

October, 2012

Abstract

Agriculture is an important economical activity in many countries that could benefit from latest technologies in order to carry out activities in a problem-orientated manner, improving the efficiency of the agricultural activity and the environmental performance. In this study an unmanned aerial vehicle (UAV) with a low cost consumer grade RGB camera were used to acquire imagery over a sugarcane plantation on the pacific coast of Nicaragua, in order to map green vegetation.

Imagery was processed and analyzed under different conditions (display scale and resolution) in order to explore the effects over the accuracy of the classification carried out by the observer and by vegetation indices. Furthermore, Stolf (1989) field methodology was adapted to be used with high resolution (4.7 cm pixel size) aerial images and the resulting gap percentage calculations were compared with vegetation cover percentage derived from the vegetation indices. In addition a record of all file sizes and processing time required was presented to help describing the limitations of such ultrahigh resolution imagery.

Findings showed an overall accuracy of the VI green vegetation estimation of 86.0% and differences in estimating green vegetation cover due to resolution change (from to 4.7 cm to 23.5cm) were not bigger than 1.1% using 5% of the data storage capacity of the original imagery. A smaller display scale (1:8 compared to 1:40) increased the number of the unknown class for validation points by the observer while it reduced the time required for validation around 20%. Gap automatic detection produced 5% differences compared to visual inspection. Later, vegetation cover and gap relation were modeled using a simple lineal regression (R^2 =0.97 at 0.05 significance level), which allowed to use Stolf classification based on gap percentage to map the area. A map to be used as a decision support tool for farmers at the specific sites and valid as the basis for precision agriculture.

Table of Contents

2.1 Introduction

Sugarcane is one of the main crops of great importance for the Nicaraguan economy covering around 25,000 ha of land in the departments of Chinandega and Leon, on the pacific coast of Nicaragua(Ramírez et al. 2010). In these areas human labor is required for many field activities e.g. for the planting process, weed removal, evaluation of gaps, harvest along the extensive plots, supervision of the activities and monitoring of the different crop stages.

Traditionally, in the early stage of the plant growth (~35 days after harvesting) the evaluation of gaps and replanting is carried out by sending a large number of people to the field (i.e. 10-20 people for a 50-80 ha plot during 2 days) in order to visually inspect the areas. These people look for and count gaps along the crop, but this process is time and labor consuming. Moreover, the whole plot is not covered since the high environmental temperature and muddy terrain, during most part of the year, severely restrict mobility along the field. Recently, a quantitative methodology for the evaluation of gaps has been implemented in some sugarcane plantations in Nicaragua. Thereby, the gaps are measured and recorded systematically allowing comparison between plots, as explained later in methodology (Stolf, R. 1986).

However, a given area presents large variations both among and within plots, thus more detailed information of the field is required to improve production, reduce costs of agricultural inputs while at the same time reducing the environmental impacts. For instance, knowing the areas with sugarcane will be useful to apply the right amount of water and not more than necessary, an important environmental aspect since sugarcane compared to other crops, requires the largest amount of water in the region (CRM 2007).

In addition, difficult environmental conditions like intense solar radiation, high temperature and humidity, as well as muddy terrain make the sugarcane plantation a harsh environment for workers. Studies have found that in Central America

agricultural workers have a higher risk for certain diseases such as chronic kidney disease (CKD) or Chronic Renal Insufficiency (CRI). Although, the causes are not totally understood yet, it has been suggested that heat stress might be one of the main risk factors(Torres-Lacourt et al. 2008).Therefore, until a better understanding of the causes of the diseases affecting agricultural workers has been reached, crop field work should be avoided as much as possible.

In order to fulfill the need for more information of the sugarcane plantations and to improve the efficiency of the agricultural human labor by introducing problem-orientated labor, remote sensing techniques have been proposed and used for different applications and with a wide variety of platforms and sensors in the last decades (Rahman et al. 1995; Xavier et al. 2006; Bégué et al. 2010). But, their use is not common due to the high costs, limitations of traditional platforms like spatial/temporal resolution, weather restrictions and the requirement for highly specialized technicians in order to transform the imagery into a useful tool for farmers.

Furthermore, while large corporations use and invest in new technologies for agriculture, the use of these technologies by small and medium size farmers is still uncommon. Due to a lack of knowledge and existing mistrust towards new technology, farmers interested in obtaining aerial images of their fields often request ultrahigh resolution images (<0.1m). This level of detail is too costly and does not add much information to the decision making process. For example, in the case of sugarcane, farmers required imagery at 4-8 cm per pixel. Such detail limits the operation, requires a lot of image processing time and produces very large files that hinder its use and storage, increasing the cost of obtaining that information and of handling it among many stakeholders.

Regarding the technology used, while multispectral sensors including near infrared (NIR) undoubtedly offers important advantages to retrieve information on crops and

thus is extensively used in remote sensing for agricultural applications, the visible part of the electromagnetic spectrum also has considerable potential.

The visible region of the electromagnetic spectrum has been used for estimates of green plant coverage with an error rate lower than 10% of corn and wheat under different atmospheric conditions(Rundquist et al. 2001; Gitelson et al. 2002), for predicting the leaf water potential of potato plants (Zakaluk and Ranjan 2008), and lately, it was also used to accurately estimate total LAI (R^2=0.97) in a maize field (Sakamoto et al. 2012).

In addition, multispectral cameras raise the cost and technical complexity of processing and operations. Furthermore, these cameras have a comparatively lower profile than commercial RGB cameras in terms of photography technology and resulting image quality. Considering also the difficult landing conditions for UAVs and the wide range of applications, conventional RGB digital cameras are a sensible choice nowadays.

Besides the sensor, the platform plays an important role since conventional ones such as satellite and manned aircraft have weather limitations and their cost is only justified when large extensions are to be cover. In the case of the application for sugarcane in Nicaragua, this wouldn't be appropriate since many plots in the same area have a different growth stage and thus need to be monitored at different times. Thus, the use of UAV promises to be a good platform for monitoring activities of small plots in a regular manner.

The objectives of this research were: 1. To identify and estimate green vegetation cover from RGB imagery obtained with a low cost consumer grade camera and a UAV platform. 2. To Analyze the effect of two different spatial resolutions and display scale on the identification and estimation of green vegetation cover in terms of accuracy and required processing time. 3. To adapt STOLF field method to aerial imagery to evaluate gaps in sugarcane plantations and compare it with the proposed

methodology for identification and estimation of green vegetation cover.

2.2 Methods

2.2.1 UAV, Sensor and Image Acquisition

A Cropcam UAV (http://www.cropcam.com) was used for aerial image acquisition (**Figure 2.1**). The Cropcam weighs 3 kg, has a wingspan of 1.8 m and a theoretical endurance of 45 minutes. In practice due to payload weight, wind speed and airframe modifications for a more stable flight and safe landing, endurance is reduced to an effective 20 minutes of flying at an average speed of 60km/hour (Evolo Co. unpublished data). It contains a military grade autopilot unit (MP2028) ,which is a electromechanical system used to guide the plane without assistance from a human being, in a radio controlled glider airframe. The autopilot guide the plane using GPS technology and differences in air pressure with a pitot tube in order to improve the speed control, flight performance and stability. It has telemetry capacities, and transmits its position (x,y,z) to a ground station using a radio modem and a computer, allowing the user to control the plane either via the radio control transmitter or via the ground control station. The autopilot supports multiple features and is programmable to fly a pattern at a specific altitude and trigger a camera or other payload at specific locations(Cropcam manual). On the ground, the UAV is controlled using HORIZON ground control software (Micropilot Co., Canada).

Figure 2.1: Cropcam UAV used for image acquisition over sugarcane fields[1]. *(Cropcam Image* 2012)

The cropcam was equipped with a consumer grade still camera, a Canon SD780is (**Figure 2.2**) 12.1 mega pixels, with 5.9 mm focal length and a 1/ 2.3" CCD sensor (6.17x4.55mm) that was carried under the wing.

Figure 2.2:. Camera Canon SD780is[2]. **(*Canon SD780 Camera* 2012)**

The flight mission was planned with Lentsika software(http://www.lentsika.ceped.it) which transformed the overlaps and pixel size requirements into flight commands and parameter information for the autopilot. However, Lentsika software does not take

1Image taken from http://www.barnardmicrosystems.com
2Image taken from http://www.digitalcamerareview.com

into account specific camera features that are required to accomplish an accurate pixel size estimation so further calculations had to be made and the Lentsika information was used only as a rough estimation.

The UAV imagery was acquired in a private sugarcane plantation located in Leon department, Nicaragua (**see Figure 2.3**). In this region, Evolo S.A., a company working in UAV operations for agricultural applications, has been testing and adapting different systems for local conditions. For the images under study, a 16 min flight was carried out in November, 2011 covering 40 hectares of *El Gobierno* plot with an average pixel resolution of 4.7 cm. Later, a mosaic was created using a stitching software in a period of 3 hours obtaining a single file (50 Mb).

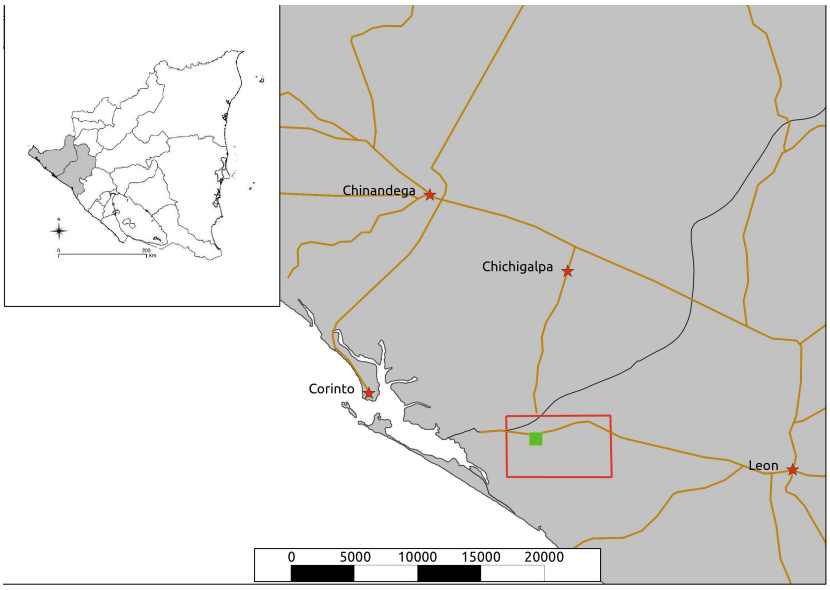

Figure 2.3: Location of UAV images acquisition in Leon Department, Nicaragua

2.2.2 Image Processing

In this research, a mosaic file was provided by the company Evolo and our focus was on the processing and analysis of the information related with green vegetation cover which was performed using open source softwares such as Quantum GIS (version 1.7.4) and R (version 0.96.330) for statistical analysis, data manipulation and image transformation. A summary of the workflow to estimate green vegetation cover is presented in **Figure 2.4.**

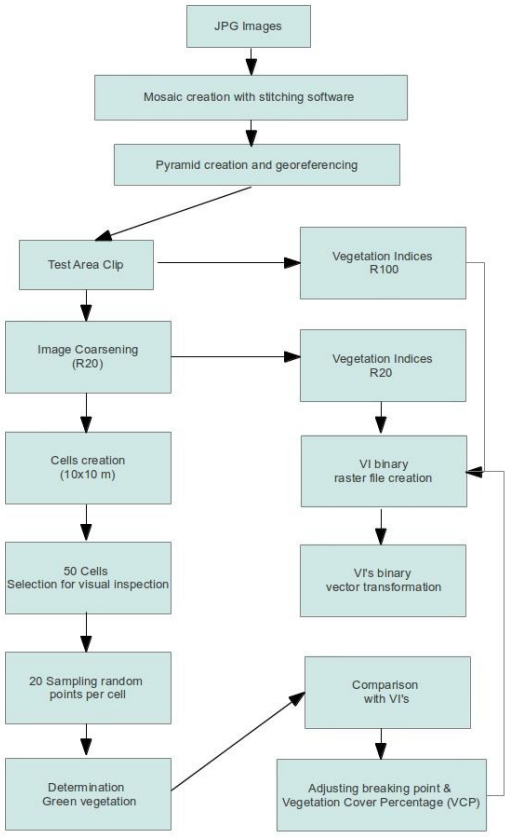

Figure 2.4: Workflow of image processing to obtain green vegetation cover.

2.2.2.1 Pyramid Creation and Georeferencing

Pyramid created a hierarchical file with different resolutions for fast image display using the *Build Overview Tool* (**Figure 2.5**) in QGIS. Despite obtaining a larger file (10269x6216 pixels, 287Mb) after the pyramids compared to the original (20538x12432 pixels, 52 Mb) file, the pyramid process increased the speed of display.

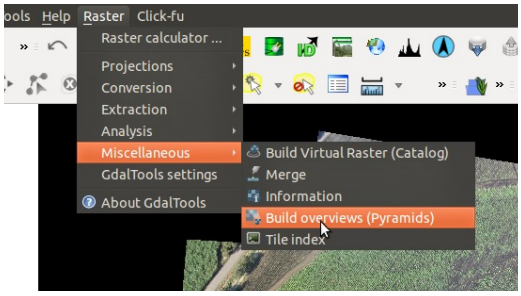

***Figure 2.5**: Pyramid creation using the Build Overview Tool in QGIS*

Georeferencing was performed using the *Georeferencer Tool* with 4 control points and a first degree polynomial transformation. This transformation was used because the terrain was flat and the area small (40 ha).

The computer processing required 10 min and produced a file (20774x13300 pixels, 829 Mb) with 4.7 cm pixel resolution with an average residual error of 45 pixels, equivalent to 2.12 m.

2.2.2.2 Test Area Clip and Image Coarsening

In order to set up and test our methods for vegetation cover estimation and gap measures, we selected and area of interest of 8.3 ha at the southwestern part of El Gobierno plot (**Figure 2.6)** and saved as a different file (5941x6272 pixel ,112 Mb) at original resolution (R100) using the *Clip Tool* in QGIS.

Figure 2.6. Test area marked with red was extracted using the Clipper tool.

Afterwards, in order to evaluate the effect of using different image resolution, the test image was coarsened using the *Translate Tool* from Raster/Conversion in QGIS. In this image transformation, pixel size was increased from 4.7cm to 23.5cm (**Figure 2.7**) and the total number of pixels was reduced in 80% of the image (R20) covering the same area (1305x1411 pixel, 5.5 Mb).

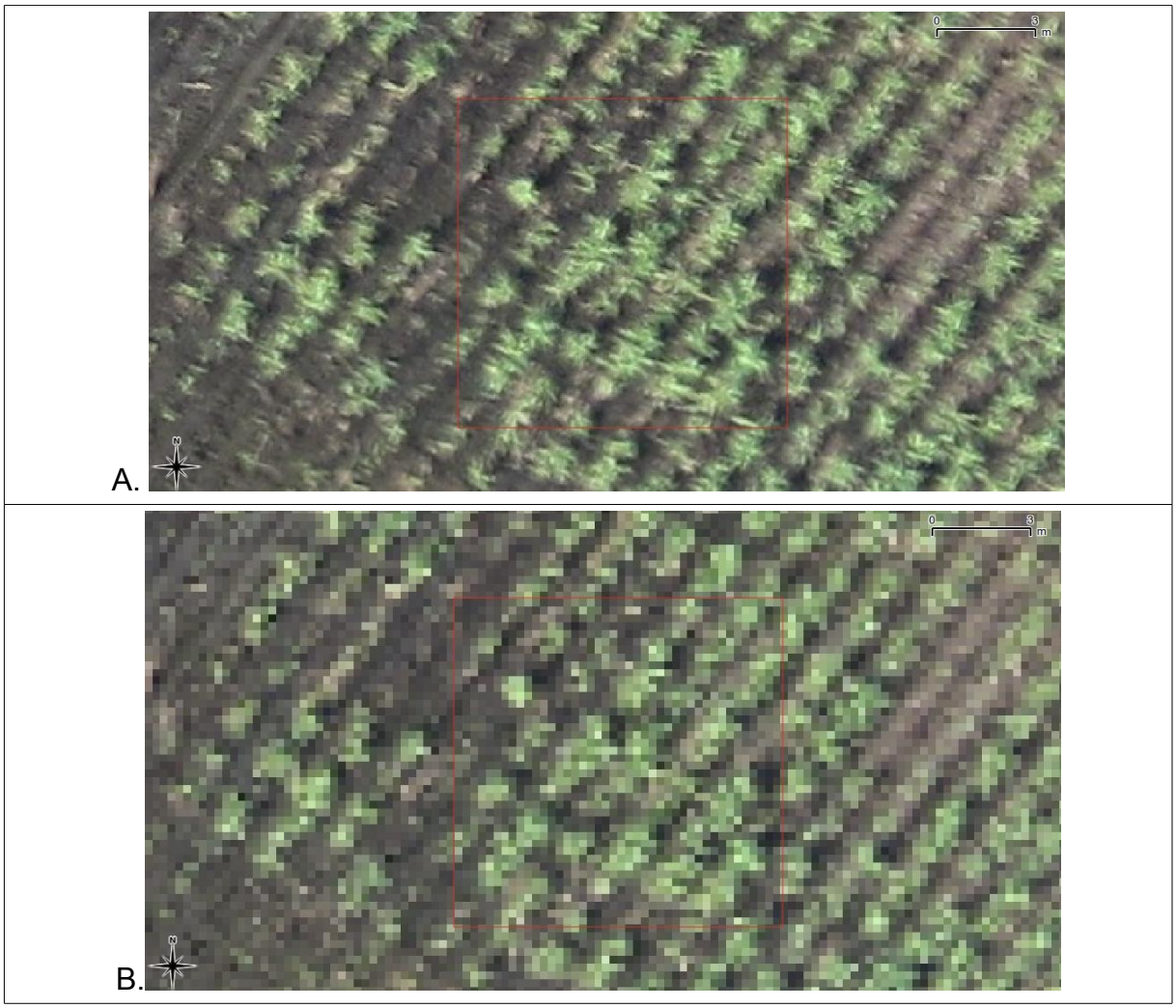

Figure 2.7. A. Original resolution (R100) and coarsened resolution (R20). Scale 1:100.

2.2.2.3 Vegetation Indices

Several vegetation indices have been proposed for the visible part of the spectrum such as simple ratios, normalized differences between bands and others taking atmospheric corrections into account (Zakaluk and Ranjan 2008). Here, three vegetation indices were used to estimate the green cover and the algorithms to calculate them are presented in **table 2.1**.

Table 2.1. *Vegetation Indices equations.*

Name	Equation / Conditions	Observations
VI-1	200* (G-R)/(G+R)	G= Green band digital number R = Red band digital number B=Blue band digital number
VI-2	200* (G-(R+B)) / (G+(R+B))	
VI-3	VI-3=1 if VI-1bin=1 & VI-2bin =1. Otherwise, VI-3=0	Binary index created from VI-1 and VI-2 binary files.

These vegetation indices were calculated for each pixel of the test area at original (R100) and coarse resolution (R20). Resultant vegetation indices images were converted in R to binary files using threshold values in order to classify the area in vegetation and ground. Threshold values were estimated by simple observations of vegetation and their VI values, using 0 for VI-1and 6 for VI-2.

Using VI-1 and VI-2 information, VI-3 classified a pixel as vegetation only when both indices (1 and 2) had classified as such, otherwise it would be represented as ground. For all VI binary files, vegetation is represented with white color (DN=1) and ground as black (DN=0).

2.2.2.4 Validation data and Vegetation Indices

A grid of 10x10 m was created for the test area with the vector-grid tool obtaining 840 cells for an area of 300x 280 m. A set of 50 cells were randomly selected and a subset (15/50 cells) was used for the validation of vegetation indices (**Figure 2.8**). In each of these 15 cells, 20 random points were generated producing a total of 300 points where visual inspection was performed and class was recorded. The data obtained from the observation was considered as validation data.

Based on a binomial probability distribution, known sample size (300 points) and a expected percent accuracy of 90%, an error of 3.46% it was estimated using the following formula (Fitzpatrick-Lins, 1981).

$$N = \frac{(Z^2)(p)(q)}{E^2} \quad \text{->} \quad E = \sqrt{\frac{(Z^2)(p)(q)}{N}}$$

In the formula p is the expected percent accuracy of the entire map, q=100-p, E is the error, and Z=2 from the standard normal deviate of 1.96 for the 95% two-sided confidence level.

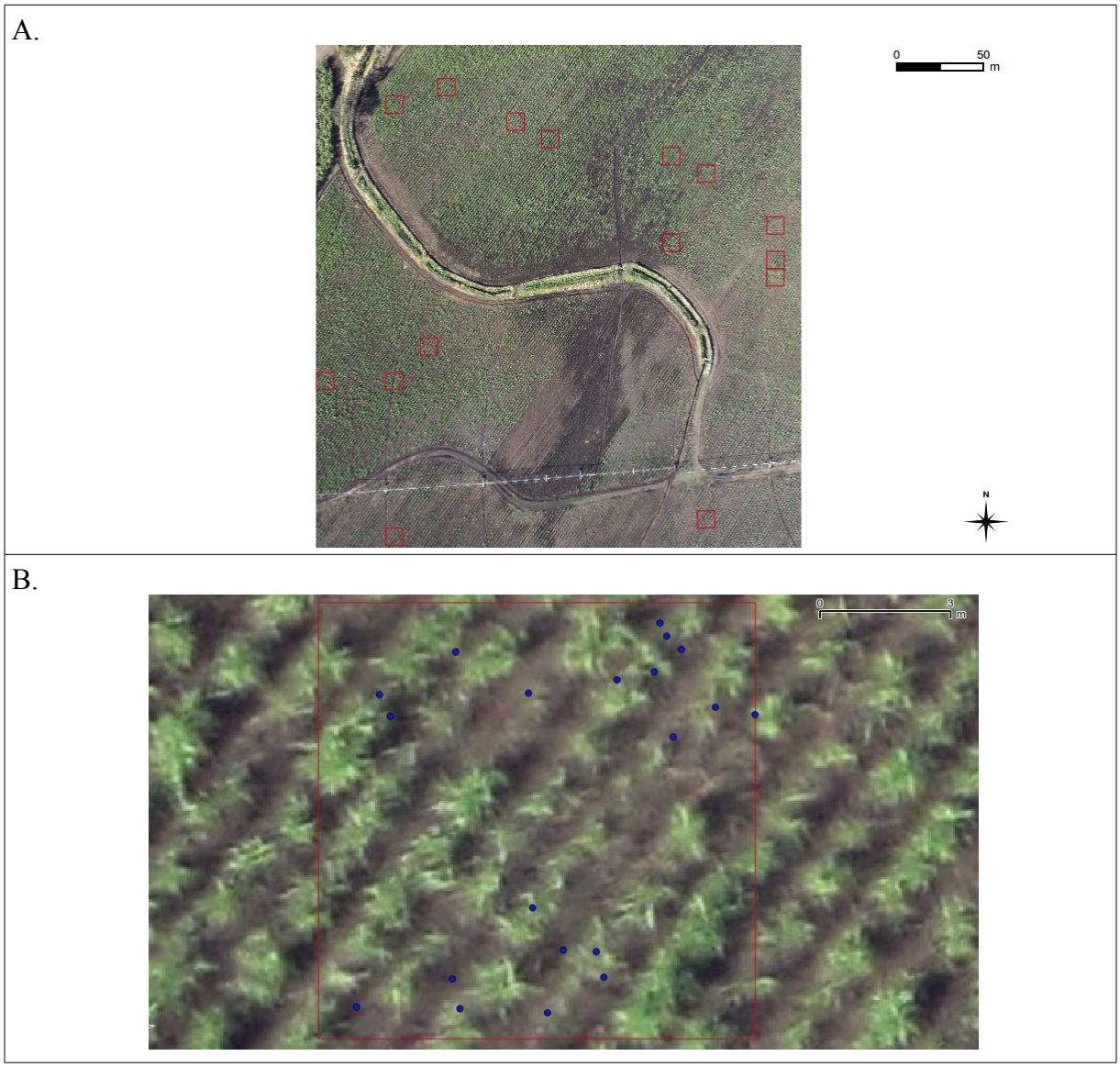

Figure 2.8. Cells for validation in red (A) and validation points in blue within one cell (B).

Validation data was generated using the original full resolution RGB image (R100 at display scale 1:8) for each point (300 points in total), where classification by visual inspection was carried out into three classes (green vegetation, ground and unknown). This procedure was repeated at a display scale(1:40) and later with coarse resolution image(R20) in order to explore the effect of display scale and image resolution on the time required and on the percentage of correct classification by visual inspection using the validation data as the reference. In other words, it was tested how using two different display scales and two resolutions would affect the accuracy of the classification done by the observer and the time required to do so.

Information from the vegetation indices and the RGB image was extracted at the 300 sites from the different resolution (R100 and R20). This procedure was carried out using the *Point-Sampling Tool of QGIS.*

The data from observations was compared with the VI data (values and classification) from the point sites, where the percentage of correct estimations by the VI model was recorded. Later the necessity to adjust the thresholds was verified by selecting the one with less errors in classification and inspecting the changes compared to the RGB image.

Vegetation cover Percentage (VCP) was computed using VI-3 and the grid vector through R, where the mean value in the binary file in one cell was equivalent to the percentage of green cover for that cell. In addition, median and median absolute deviation (MAD) were calculated for the vegetation indices within each cell to explore whether the median itself could be used as an indicator of vegetation cover.

After the selection of the VI thresholds, the produced binary binary raster image was transformed to a vector which allowed multiple interaction for studying the plot and gaps along croplines.

2.2.2.5 Stolf Methodology for Gap Evaluation

Stolf (1986) proposed a methodology which states that 0.5 m is the optimum gap size above which gaps should be measured for comparison purposes in different areas. To carry out the gap evaluation, it is necessary to count and add the total meters of gaps above 0.5 m, measured between the base of the stem (**Figure 2.9**). To do so, a measuring tape and a 0.5 m stick are required, which in case of doubt define whether the gap is larger or shorter than this value. The gap length is accumulated and then the number, and more importantly, the percentage of gaps in a given distance is reported.

In addition, Stolf found that 0.5 m is a robust measure for gap evaluation and proved that changes in the range (0.4-0.6 m) do not represent an important effect in the percentage of gaps reported for the same plot (Stolf, R. 1986).

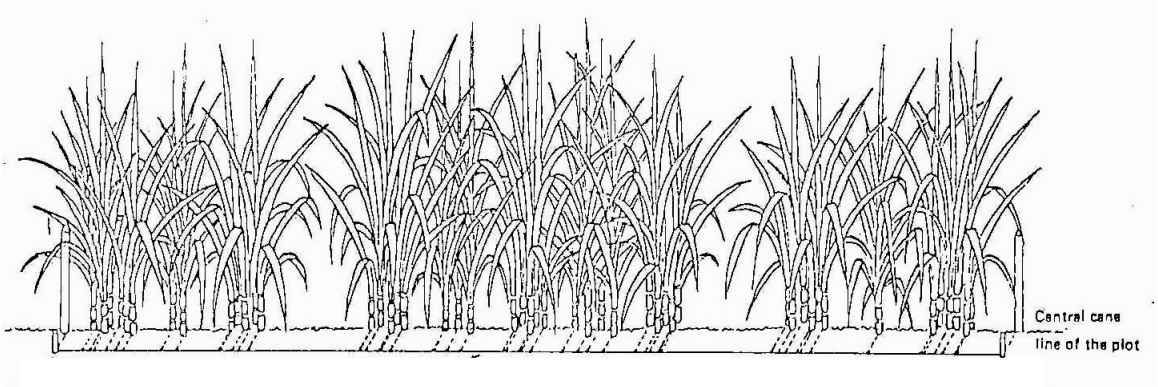

Figure 2.9. Sugarcane cropline and projection to straight line. The distance is measured between the base of consecutive stems. Image taken from Stolf (1986).

For a better comparison between different plots and conditions, Stolf (1989) also proposed a classification according to the different ranges of gap percentages and some observations related to crop managing decisions(**Table 2.2**).

Table 2.2. *Stolf Classification for evaluation of planting results.*

Gap Percentage	Planting Quality	Observations
0-10	Excellent	Exceptional germination conditions
10-20	Normal	Most common type observed
20-35	Subnormal	
35-50	Bad	Possibility of renewal may be considered
>50	Very bad	Renewal/Replanting

In this study, Stolf methodology was adapted to high resolution aerial imagery using the same areas for validation of vegetation indices. For this purpose, a vector line was created along the center of each cropline within the 10x10 m cells (**Figure 2.10**).

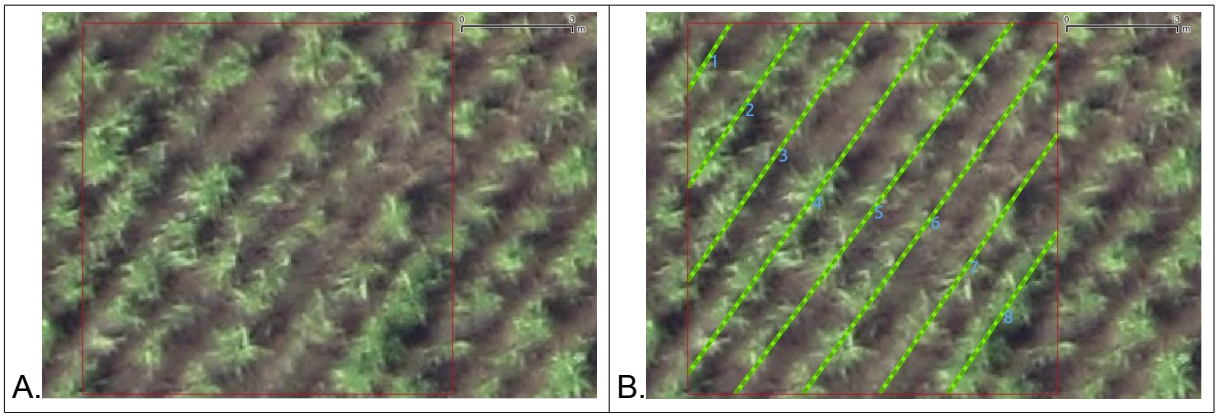

Figure 2.10. Sugarcane croplines within a validation cell (A) and lines (B), scale 1:70

Using these lines, points were created every 5 cm using the *Profile- From-Line tool* in QGIS and 20,096 points were obtained from which information (line ID, and RGB and VI values) was extracted from the different layers.

Finally, a program was created in R to automatically detect gaps based on the VI's threshold and on the length of the gaps. In this study, a gap was considered to have a minimum number of 11 continuous points, which equals to 55 cm. The program

returned the number and location of gaps per cell.

2.3 Results and discussion

2.3.1 Vegetation Indices classification and validation

The test area was classified into ground and vegetation using the different vegetation indices and the result was validated by observations for each of the sites. In **table 2.3**, a summary of the results in percentage of correct classification and observations at point sites is presented by each VI and for each condition tested.

Table 2.3. Result of Vegetation Indices Classification under different conditions and Observations.

Conditions		Estimation	Vegetation Indices Performance (%)			Observations		
Resolution	Display Scale		vi1b	vi2b6	vi3b	Vegetation	Ground	Unknown
R100	1:40	Correct	76.33	78.00	78.67	171	88	41
		Incorrect	10.00	8.33	7.67			
	1:8	Correct	79.00	85.67	86.00	166	133	1
		Incorrect	20.67	14.00	13.67			
R20	1:40	Correct	74.67	77.67	77.67	119	153	28
		Incorrect	16.00	13.00	13.00			

Under Observations (right side of **table 2.3**), the number of points per class is shown where unknown class points were not considered as part of the incorrect estimations since the VI is bimodal and can classify only into ground or vegetation. Under the Vegetation Indices Performance, there are three columns, one for each binary VI used and the values represent the percentage of points that were classified under correct and incorrect class when compared to observations.

Besides the percentage of accuracy to evaluate the effect of using a given VI with a specific threshold, images of the test site were visually inspected and compared.

2.3.1.1 Vegetation Indices Comparison

VI-1 presented some problems when low light conditions occurred in the scenery, taking shaded soil as vegetation while vegetation was correctly identified, which produced an over-estimate of the vegetation cover (**Figure 2.11**), a phenomenon reported before (Gitelson et al. 2002). Due to the different light conditions in which the UAV systems needs to operate, this misclassification was not acceptable.

VI-2 eliminated the problem of recognizing non-vegetated shaded cover as vegetation, using the blue band information that take into account the different light conditions as it has been used in other vegetation indices (Wu et al. 2007; Payero et al. 2004; Gitelson et al. 2002; Qi et al. 1994) . However, VI-2 classified some areas as vegetation where there was none.

VI-3 which only classified vegetation when VI-1 and V-2 both classified and area as vegetation produced the best results in terms of overall accuracy.

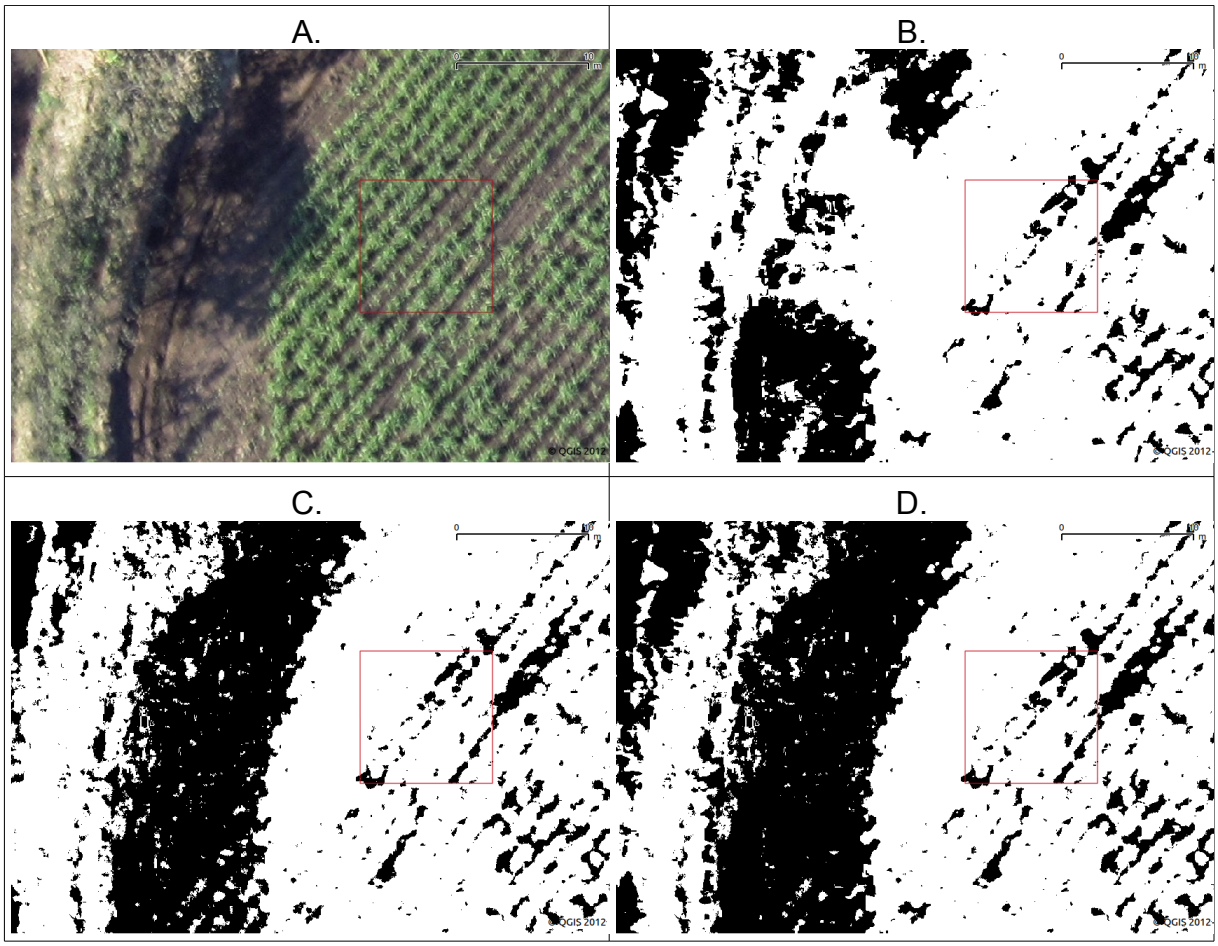

Figure 2.11**.** Classification of vegetation by different VI at low light conditions. Vegetation (white) and ground (black), scale 1:200. A. Original RGB image (R100), B. VI-1 classification, C. VI-2 classification and D. VI-3 classification.

The observations at the highest resolution (R100) and the largest display scale were considered as the true classification of the point´s sites. This data was compared to the VI-3 with an overall correct classification of 86% and a confusion matrix was obtained (**table 2.4**).

Table 2.4 *. Confusion matrix for maximum resolution (R100) with the larger display scale (1:8)*

R100display scale 1:8			
Predicted Class by VI-3	Observed		
	Ground	Vegetation	Unknown
Ground	97	5	1
Vegetation	36	161	NA

An evaluation of the confusion matrix revealed an overall accuracy of 86% and the correspondent accuracies from the producer´s and user´s perspective (**table 2.5**). The producer's accuracy indicates the probability of a reference pixel being correctly classified while the user's accuracy is the probability that a pixel classified on the map actually represents that category in reality (Story and Congalton 1986).

Table 2.5 *. Evaluation of Confusion Matrix*

Category	Producer`s Accuracy	User's Accuracy
Ground	0.73	0.94
Vegetation	0.97	0.81

In order to better understand the cause of errors for VI-3 from the producer point of view, histograms for correct, incorrect, vegetation and ground class estimated by VI-1 and VI-2 are presented in **Figure 2.12.**

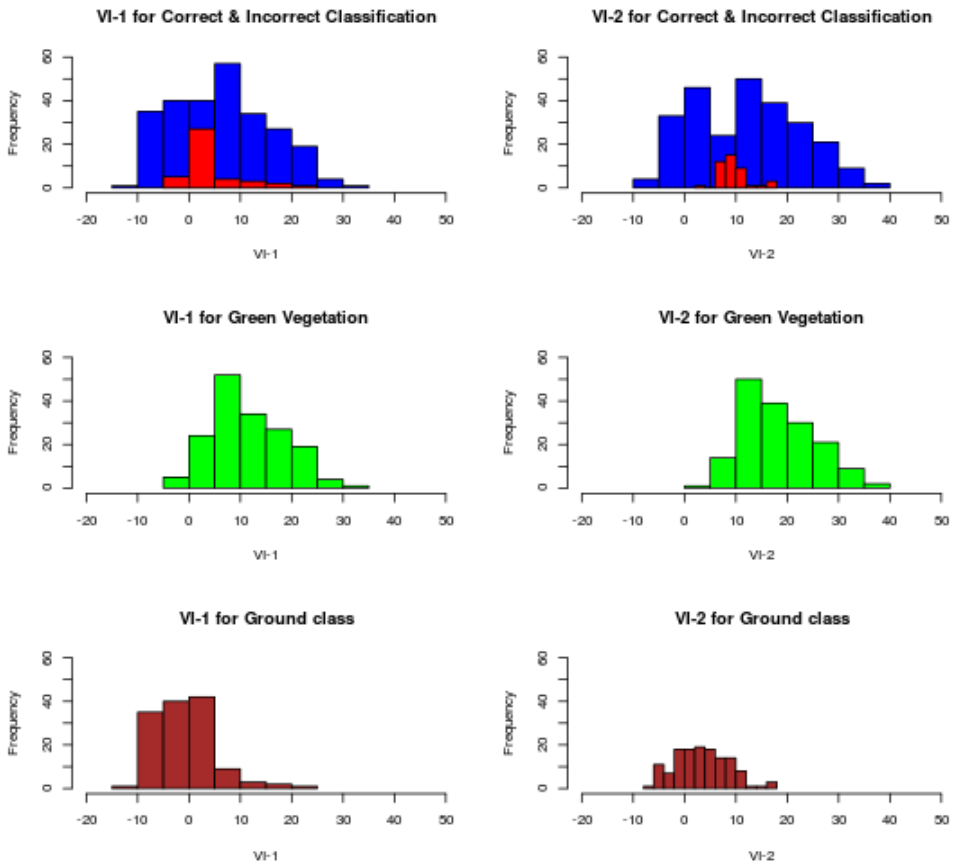

Figure 2.12. Sugarcane Histograms for different classes. On the left side VI-1 histograms and VI-2 is presented on the right side. First row are histograms for correct (blue)and incorrect (red)classification of VI compared to observations. Second row are histograms for green vegetation (green) based on observations and the third row are histograms for ground class (brown) .

In VI-1, most classification errors presented values between 0-5 and there is an overlap for vegetation and ground values around 0. While in VI-2, most classification error presented values between 5-10 with an overlap for green vegetation/ground values around 5 and with a more clear bimodal distribution than in VI-1. More detailed descriptive statistical information of the erroneous classified points can be seen in **table 2.6**.

***Table 2.6.**. Statistics for 42 points erroneously classified when matching reference data and VI-3 classification*

Statistics parameter	VI-1	VI-2
Min	-4.7	3.37
1st Quartile	1.96	7.67
Median	3.12	8.80
Mean	4.52	9.46
3rd Quartile	4.39	10.54
Max	23.16	17.44

As the maximum value with 23.16 for VI-1 and 17.44 for VI-2 were clearly outliers, the involved points (point 20, polygon 89) were revisited, finding that these pixels had very low RGB values (42,53 and 47) and the visual aspect of those pixels was very dark (**Figure 2.13**) and thus they were classified as ground by the observer.

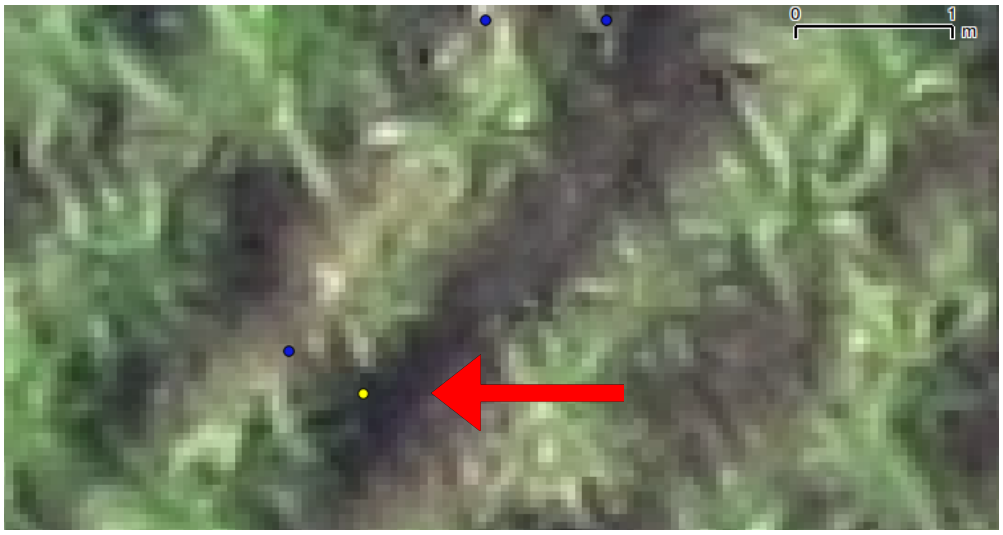

Figure 2.13. Erroneous classified point with max. value for VI-1 and VI-2. The point of interest is yellow in a dark zone of the image (scale 1:30).

2.3.1.2 Different Display Scales for Visual Inspection

In **table 3**, the number of point sites classified as vegetation, ground and as unknown can be seen. It can be noted that: a) 13.6 % of observation were (41/300 points) unknown values when working at the maximum resolution (R100) and the display scale was 1:40. The cause for this unknown values was mainly the display scale of analysis. Most of unknown class points were located close to the boundaryt between two pixels where one of them was vegetation and the other was ground. When the display scale was increased to 1:8, only one (1/300points) unknown value was registered, and in this case the reason was low brightness which made the recognition difficult.

In addition, the percentage of correct estimations also increased when the display scale increased (**table 2.7**). These finding suggest that the display scale used for visual inspection affects the percentage of correct estimations by the different VI.

Table 2.*7. Changes in correct green cover estimation under different conditions*

Conditions	Percentage of correct classification by VI		
	vi1b	vi2b6	vi3b
Resolution R100 and different display scale (1:40 to 1:8)	2.6	7.6	7.3
Same ratio display scale:Pixel-size and different Resolution (D20P to R100)	4.3	8.0	8.3

2.3.1.3 Different Spatial Resolution

When the resolution was increased from R20 to R100, the percentage of correct estimation by the VI also increased by 8.3 %. Comparing between the display scale and spatial resolution, both have similar effects increasing the percent of correct estimations but increasing the resolution increased more this percentage than the display scale.

It has to be noted that imagery with a lower resolution has a larger pixel size. Therefore, the validation strategy applied above is rather limited since the same position can have different pixel values depending on the size and surrounding pixels. In **Figure 2.14**, the effect of less resolution on the imagery VI-3 can be seen where the objects are less sharp and lines are less smooth. In addition, when only few pixels represent vegetation at maximum resolution (R100), they do not appear in the images with lower resolution (R20) since the re-sampling method used with gdal_translate package only takes 20 percent of the pixels into account and thus small objects have higher chances to disappear than larger ones.

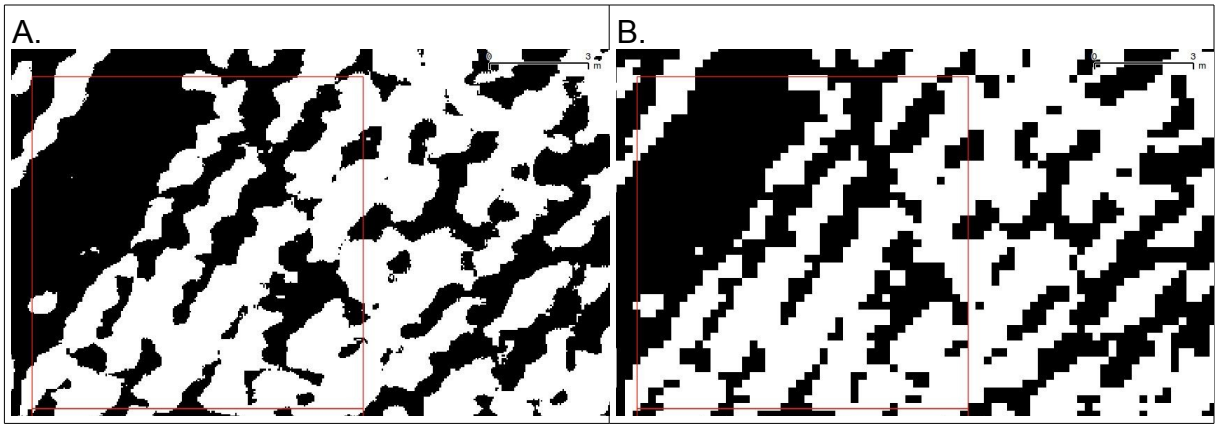

Figure 2.14. Effect of different resolutions on VI-3 layer. R100 (A) and R20 (B) (scale 1:100).

Thus, the difference in Vegetation Cover Percentage (VCP) calculated for the validation cells (10x10 m) is more important than the single pixel classification based

on VI values as described before. The difference in VCP using VI-3 is presented in **table 2.8**. The difference between VCP calculated at the different resolutions is less than 0.5 % for most cells and it is of 1.06 % when the VCP has the lowest value (24.6 %). These findings indicates that changing the resolution from 4.7 cm to 21 cm does not affect the estimation of Vegetation Cover Percentage significantly.

***Table 2.8**. Difference in VCP calculated from different spatial resolutions (R100 and R20).*

ID	Vegetation Cover Percentage (%)		R20-R100 (%)
	R100	R20	
89	87.52	87.61	0.09
533	64.75	64.20	-0.55
64	85.52	85.59	0.08
329	65.67	65.72	0.05
391	59.77	60.01	0.23
483	63.29	63.05	-0.24
219	75.15	75.39	0.24
189	86.63	86.99	0.36
363	51.31	51.03	-0.28
537	67.80	68.13	0.33
789	33.69	33.51	-0.19
307	54.10	54.27	0.18
154	80.75	81.16	0.40
124	72.17	72.57	0.40
779	24.61	25.67	1.06

Comparing the Vegetation Cover Area (sq.m) calculated for each VI resulted in a higher estimation by VI-1 of 4.45% comparing to VI-3 estimate, even though the test area presented uniform light conditions (**table 2.9**).

***Table 2.9**. Vegetation cover estimation of the validation area (1500 sq. meters) by different indices.*

Vegetation Cover Area (sq. m)	VI-1	VI-2_6	VI-3
	1041.68	1028.71	974.89

In addition, percentage of point sites classified as vegetation by the observer was compared with the VCP for each cell and a linear relation was found (**Figure 2.15**). This result was expected because there is a higher probability to find vegetation at

point sites when the Vegetation Cover Percentage is high than when it is low.

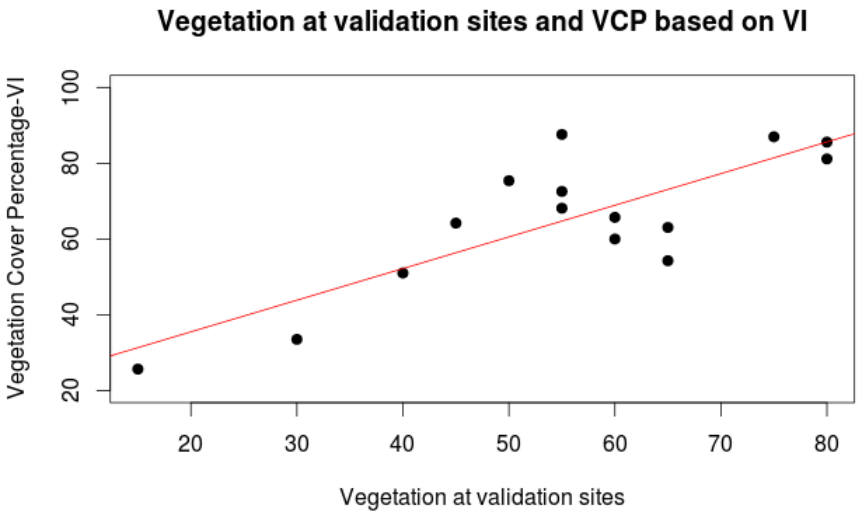

Figure 2.15**.** Comparison of Vegetation Cover Percentage for 15 cells estimated with VI-3 vs Vegetation Percentage of point observation sites using R100 (display scale 1: 8).

2.3.1.4 Threshold Adjustment

In order to evaluate the thresholds as the optimum breaking points, lower and higher values than the originally chosen were tested and the number of errors produced compared to observations were counted (**table 2.10**). Points that were considered as vegetation by the observer but are classified as ground by their low VI values are labeled as Vegetation-low and points considered as ground by the observer, but are classified as vegetation according to their high VI values are labeled as Ground-high.

***Table 2.10**. Threshold values and errors of VI classification based on observations at scale 1:8*

VI	Threshold value	Vegetation-low	Ground-high	Total Error
VI-1	-0.5	3	65	68
	0	5	57	62
	0.5	5	57	62
	1	7	51	58
VI-2	5	1	50	51
	6	1	41	42
	7	1	35	36
	8	6	27	33

It was found that the total number of errors for VI-1 decreased when the threshold value increased until it was 1. However, after comparing the differences in the binary image created by each threshold, 0 was selected as the optimum threshold for VI-1, which was the one already used for creation of vegetation cover binary file.

Error values for VI-1 were explored using 0 as threshold and the majority (30/57) of the Ground-high errors had green band values lower than 100 and the rest of the points classified as Ground-high (27/57) had low differences between the green and red band.

In the case of VI-2, the minimum number of total errors was obtained when the threshold value was 8 with 33 errors. However, after comparing the effects of the different thresholds it was decided to keep using the value of 6 as optimum threshold since it was noted that certain areas with green vegetation were not considered as such when using a value of 8.

This conflict in the criteria for selecting the best threshold can be explained with the fact that there is an overlap of VI values between pixels considered as vegetation and ground by the observer (**Figure 2.12**). This overlap between classes was lower for VI-2, but, in any case, pixels with VI values within these range cannot be reliably classified as vegetation or ground. It is important to note that the observer does not only use the color of the target pixel for classification, but also the color of surrounding pixels and depending of the color of these surrounding, the target pixel

appears as vegetation or ground to the observer. Thus, a unknown class should be added to the VI model in the future.

2.3.2 Stolf Adjusted Methodology

Automatic detection of gaps was developed and minor mistakes were detected by visual inspection.. One type of error was that the vector line does not follow the cropline perfectly and since the detection methods only took into account information from the points along the line, more care should be taken at the moment of drawing the lines (**Figure 2.16**). Another error found was that gaps were considering points from different lines. This situation could be avoided using single lines for gap detection or improving the automatic detection code so it can differentiate between lines. Despite these problems, visual inspection showed around 5% differences compared to automatic results (data not shown).

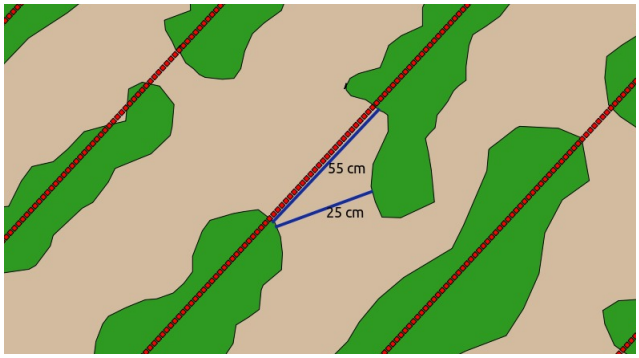

Figure 2.16. *Automatic gap detection error. Line (red) not following the shape of the cropline (green). Distance reported (blue) is the one of cropline (55 cm) considering it a gap, when it shouldn't be a gap since the distance should be measure along the closest consecutive parts of the canopy (25 cm).*

Using this approach, it should be taken into account that: 1. the field Stolf methodology is based on the distance between the base of consecutive stems, while

in this study the green parts of the plant´s canopy were used. This means that the distance of the gap based on stem would be higher than the reported with this adaptation. 2. Stolf methodology considers a gap when there is no vegetation along 0.5 m, but with proposed adaption mentioned above, vegetation that was not green was considered as ground.

Results of gap detection and VCP for each cell (**table 2.11**) showed that the total cropline distance was not constant and that the cell with the maximum VCP value(189) did not reported the minimum gap percentage. These indicates that there are different levels of plant growth along the evaluated cells. Furthermore, the relation of VCP and the gap percentage is inversely proportional as expected but the mathematical relation varies over time until the sugarcane has reached the point where it does not grow more and the canopy closure is maximum.

***Table 2.11**. Gap information of each test area and Stolf classification.*

Cell ID	No. Pts line	ADCL (m)	No. gaps >0.55 m	No. Points gap	Gaps (m)	Gaps (%)	VCP (%)	Stolf class by Gaps %
64	1399	69.95	1	17	0.85	1.21	85.59	Excellent
89	1385	69.25	3	37	1.85	2.67	87.61	Excellent
124	1341	67.05	6	110	5.50	8.20	72.56	Excellent
154	1327	66.35	3	61	3.05	4.59	81.15	Excellent
189	1345	67.25	0	0	0	0	86.98	Excellent
219	1409	70.45	1	68	3.40	4.82	75.39	Excellent
307	1466	73.30	11	318	15.90	21.69	54.27	Subnormal
329	1345	67.25	10	187	9.35	13.90	65.71	Normal
363	1340	67.00	6	316	15.80	23.58	51.02	Subnormal
391	1287	64.35	8	208	10.40	16.16	60.00	Normal
483	1309	65.45	7	132	6.60	10.08	63.05	Normal
533	1318	65.90	7	185	9.25	14.03	64.19	Normal
537	1299	64.95	6	169	8.45	13.01	68.13	Normal
779	1265	63.25	21	477	23.85	37.70	25.66	Bad
789	1261	63.05	13	409	20.45	32.43	33.50	Subnormal

Cell ID: Id for sampling cells.
ADCL: Accumulated distance for croplines

The VCP-gap percentage relation was modeled using a simple lineal regression. In **Figure 2.17** this relation is displayed with a red line representing the regression line, for which the following function was obtained with R squared of 0.97, P-value(9.158e-12) at at 0.05 significance level:

$$VC\ (\%) = 86.983 * Gap(\%) - 1.617$$

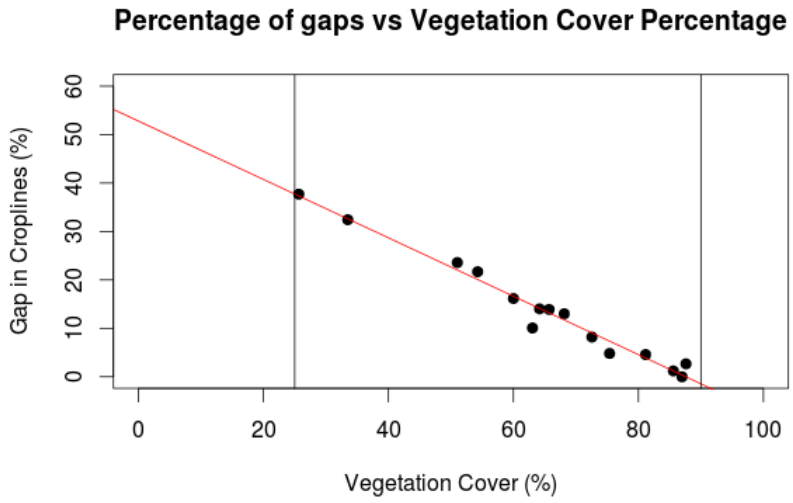

Figure 2.17. *Percentage of Gaps vs* VC percentage estimated with VI-3.

In order to test how good the regression model prediction performed, 10 new cells were selected for validation. The gap percentage and the VCP were estimated and compared to the predicted VCP using a prediction interval of 0.95 % and assuming a normal distribution of the error. As a result, 80% (8/10 cells) of the values measured by VI-3 were inside the predicted interval knowing the gap percentage (**Figure 2.18**) and the other values were very close to the interval. These results could be improved including more data to adjust the linear model and using it with vegetation at the same growth stage, since it is when the relation between gaps and vegetation cover is more stable.

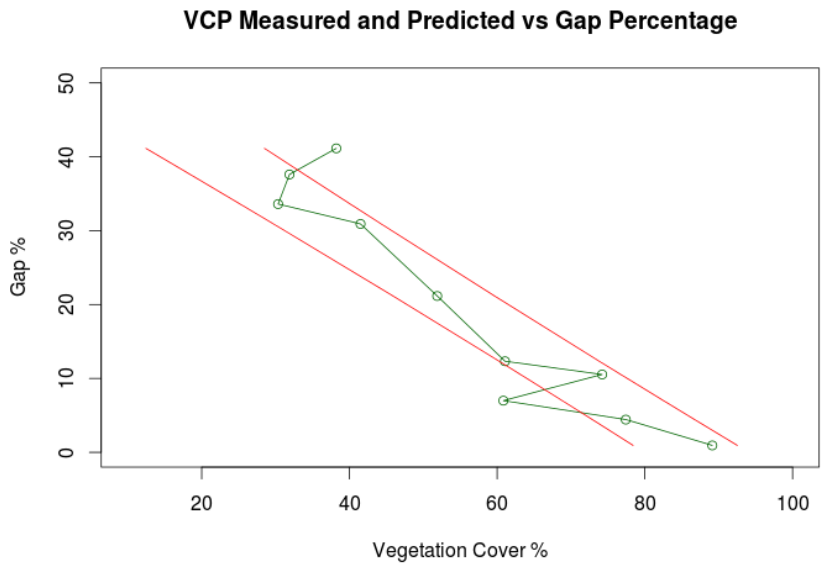

Figure 2.18. *Vegetation Cover Percentage measured with VI-3 and predicted using the gap percentage.Red lines represent the prediction interval of the VCP values and the green line is the VCP calculated with VI-3.*

As it was previously proven (in section 3.5) that the estimation of VCP between the two resolutions tested did not vary significantly (<1%), R20 resolution was used for further analysis since it requires less time for processing.

In addition, it was explored the median and median absolute deviation (MAD) of the VI for each cell as indicators of the Vegetation Cover Percentage (**Figure 2.19**). However, medians for both VI did not present a clear relation with VCP and MAD showed a high level of overlap between several VCP. Therefore, the use of the median value was not considered as a good proxy of VCP.

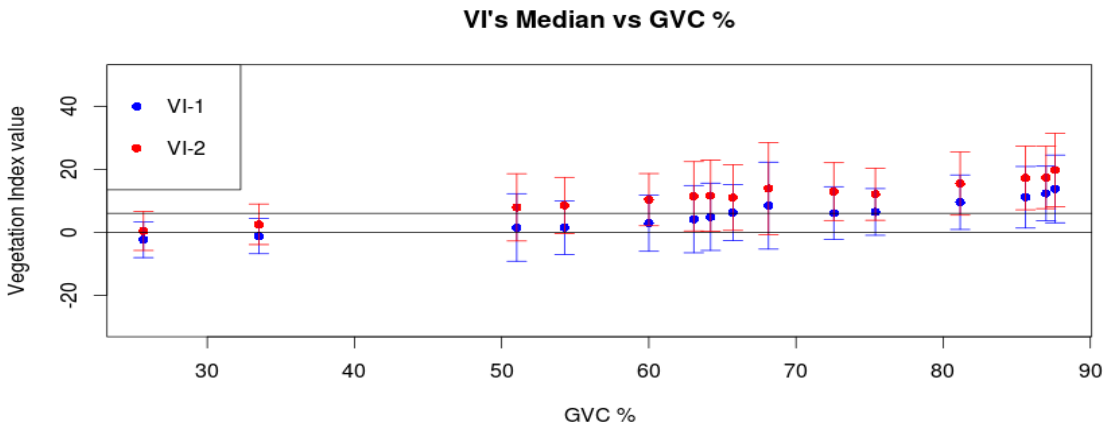

Figure 2.19. *Vegetation Indices median vs* Vegetation Cover Percentage

As a result of the test area classification and the analysis performed under different VI and conditions, it was possible to conclude two final products that could be used by the farmers.

One is a vector map (grid 10x10m) presenting the areas classified according the VCP using the same classes proposed by Stolf for percentage of gaps in each plot. To estimate the thresholds of the Stolf classification, the regression equation presented above was applied and the fit value was used with 95% confidence interval. The results are presented in **table 2.12** and the map for the test area is display in **Figure 2.20**.

Table 2.12*. Calculated VCP thresholds according Stolf gap classification*

Stolf Threshold (Gap %)	Threshold VCP % (estimated)
10	70.81
20	54.64
35	30.39
50	6.14

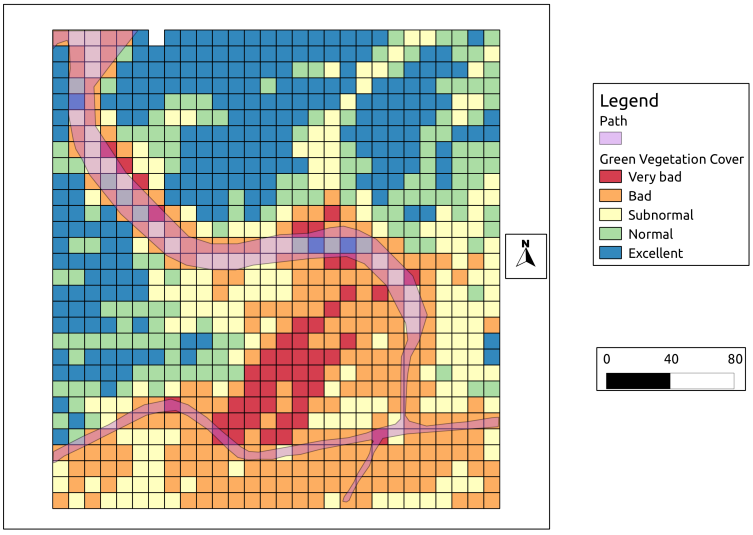

Figure 2.20. *Green Vegetation Cover Map for test area.*

Another product was a vector layer of all vegetation, which can be used together with other information (e.g. soil type and nutrients availability) to explore the causes for gaps. For example, a farmer might be interested to know the continuous areas without vegetation larger than 5 sqm (**Figure 2.21**).

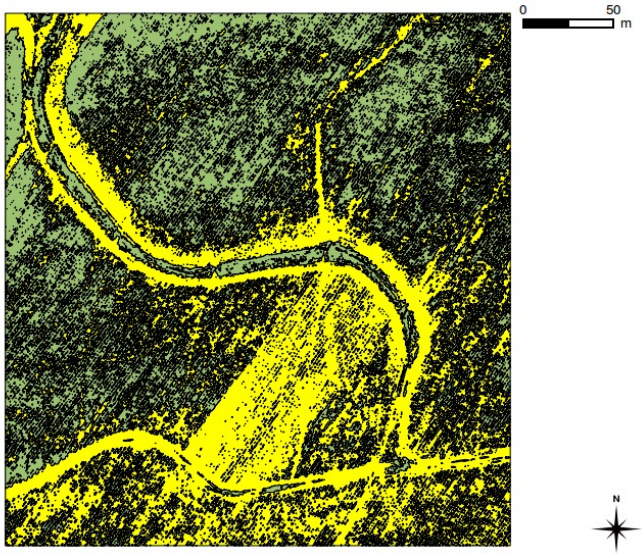

Figure 2.21. Layer of vegetation as vectors. *Continuous area without vegetation larger than 5 sq.m presented in yellow color.*

2.3.3 Processing Time and computer storage capacity

Some of the limitations found in daily application in an agricultural environment is the need for information on time and the required infrastructure to generate, share and maintain such information for future analysis between all the stakeholders. Therefore, information on average time for some of the processing steps and required digital storage capacity is provided.

The process that required most time was the visual inspection with 250 min or more (**table 2.13**). Comparing this process with the two resolutions, there was a similar time requirement of approximate 300-350 min for R100 and 250-300 min for R20, however these small differences (~50 min) are expected to become greater when the area to be processed increases.

Table 2.13. *Required processing time*

Process	Resolution	
	R100	R20
Pyramid creation for fast display	15 min	NA
Georeferencing of mosaic	25 min	NA
Creation of Test Area binary file	4-5 min	2-3 min
Creation of VI-3 (no included VI-1 and VI-2 binary files creation)	20 sec	20 sec
Extraction of 20096 points with 10 fields	25 min	NA
Statistic calculations per VI's for 1500 sq.m.	200 sec	140 sec
Visual inspection of 300 points (same ratio scale:pixel size)	300-350 min	250-300 min

In **table 2.14**, the digital storage capacity required is presented which should be taken into account when managing this kind of information and designing monitoring campaigns, producing information that is expected to be shared between different

stakeholders with different types of computer infrastructure. Comparing the two resolutions, the advantage of using R20 is clear which required only 4% of the size of the same file for R100 with the exception of the binary files which have equivalent sizes.

***Table 2.14**. Required digital storage capacity*

File	File Size (MB)	
	R100	R20
Mosaic (.jpg)	52	NA
Pyramids (.ovr)	287	NA
Georeferenced Mosaic (.tif)	919.8	33
SW_test area	111.8	4.5
Binary file created in R (tif)	4.4	4.1

Detailed information regarding the computer specifications and operative system (OS) is presented in **table 2.15**.

***Table 2.15**. Computer and OS Specifications*

Computer model	Samsung R580
Graphics Card	1Gb NVIDIA Geforce 330M
RAM Memory	4.0 Gb
Processor	Intel Core i5 520M (2.40GHz)
Operative system	Ubuntu 11.10

2.4 Conclusion

1. It was possible to identify and estimate green vegetation cover from RGB images with an overall accuracy of 86% based on point validation data using a consumer grade camera and a UAV platform.
2. The resolution can play a role for the time spent on the analysis of information and the accuracy of validation. Therefore, validation should be done with the highest resolution which in this research was of 4.7 cm per pixel.
3. Variations of vegetation cover percentage estimated between the two resolutions tested in this study (4.7 cm and 23.5 cm per pixel) are not significant (~1%) and the data suggests that variation will increase inversely with the percentage of green vegetation cover.
4. There is an inverse relation between the percentage of green vegetation cover and the percentage of gaps found in the same area.
5. The lower resolution imagery (R20) used in this study required less than 5% of the digital storage capacity than using the original resolution (R100).

2.5 Recommendations

File size and processing time should be taken into account if practical tools are to be developed for small and medium size farmers with limited infrastructure and resources. In this case, free open source software was used and the existing support groups make them an excellent option to work with.

It is recommended to use ultra-high resolution imagery (<10 cm) for validation purposes only and carry out the flight missions for Vegetation Cover Percentage estimation with lower resolution which in this case was around 20 cm producing similar results as the ones obtained with the higher resolution (4.7cm).

2.5 Future Research and Challenges

It would be of great interest to:

1. Calibrate Stolf methodology used in this research with field data and evaluate its use with other crops.

2. Investigate how different types of soils and humidity conditions could be taken into account to produce more accurate results.

3. Evaluate how farmers could reduce the amount of agricultural inputs, their costs, while increasing productivity and improving their environmental performance using UAV imagery as a basis for precision agriculture.

4. Develop procedures to calibrate digital numbers of the imagery based on the position of the sun at the time of the flight.

5. Evaluate improvements in sugarcane monitoring using multispectral sensors and explore different geometric corrections methodologies required over rugged terrains.

2.6 References

Bégué, A., V. Lebourgeois, E. Bappel, P. Todoroff, A. Pellegrino, F. Baillarin, and B. Siegmund. 2010. "Spatio-temporal Variability of Sugarcane Fields and Recommendations for Yield Forecast Using NDVI." *International Journal of Remote Sensing* 31 (20) (October 15): 5391–5407. doi:10.1080/01431160903349057.

Canon SD780 Camera. 2012. Accessed June 20. http://www.digitalcamerareview.com/assets/23641.jpg.

CRM. 2007. "Plan de accion de cuencas de la región León y Chinandega". Cuenta Reto del Milenio. http://www.cuentadelmilenio.org.ni/cedoc/02negrural/05%20Conglomerado%20Forestal/01%20Documentos%20Normativos/15%20Plan%20de%20Accion%20Cuencas%20de%20Occidente%20GFA.pdf.

Cropcam Image. 2012. Accessed May 27. http://www.barnardmicrosystems.com/Pictures/a%20Cropcam%20DSC_6665%20V2.jpg.

Fitzpatrick-Lins, K. 1981. "Comparison of Sampling Procedures and Data Analysis for a Land Use and Land Cover Maps." 47 (3): 343–351.

Gitelson, A., Kaufman, J., Stark, R., and Rundquist, D. 2002. "Novel Algorithms for Remote Estimation of Vegetation Fraction." *Remote Sensing of Environment* (80): 76–87.

Payero, J. O., C. M. U. Neale, and J. L. Wright. 2004. "Comparison of Eleven Vegetation Indices for Estimating Plant Height of Alfalfa and Grass." *Applied Engineering in Agriculture* 20: 385–393.

Qi, J., A. Chehbouni, A. R. Huete, Y. H. Kerr, and S. Sorooshian. 1994. "A Modified Soil Adjusted Vegetation Index." *Remote Sensing of Environment* 48 (2): 119–126.

Rahman, M. R., A. H. M. H. Islam, and M. A. Rahman. 1995. "NDVI Derived Sugarcane Area Identification and Crop Condition Assessment." *Dept. of Geography and Environmental Studies, University of Rajshahi Bangladesh*. http://ftp.ida.liu.se/~746A27/Literature/NDVI%20derived%20sugar%20cane%20area%20identification.pdf.

Ramírez, D., J. L. Ordaz, J. Mora, A. Acosta, and B. Serna. 2010. *Efectos del Cambio Climático sobre la Agricultura, Nicaragua*. Mexico: Comisión Económica para América Latina y el Caribe (CEPAL). http://www.ruta.org:8180/xmlui/handle/123456789/758.

Rundquist, D., A. A. Gitelson, D. Derry, J. Ramirez, R. Stark, and G. P. Keydan. 2001. "Remote Estimation of Vegetation Fraction in Corn Canopies." http://digitalcommons.unl.edu/natrespapers/274/.

Sakamoto, Toshihiro, Anatoly Gitelson, Brian Wardlow, Timothy Arkebauer, Shashi Verma, Andrew Suyker, and Michio Shibayama. 2012. "Application of Day and Night Digital Photographs for Estimating Maize Biophysical Characteristics." *Precision Agriculture* 13 (3): 285–301. doi:10.1007/s11119-011-9246-1.

Stolf, R. 1986. "Methodology for gap evaluation on sugarcane lines." *STAB, Piracicaba* 4 (6) (July): 12–20.

Story, Michael, and Russell Congalton. 1986. "Accuracy Assessment - A User's Perspective."

Photogrammetric Engineering and Remote Sensing 52 (3) (March): 397–399.
Torres-Lacourt, C. et al. 2008. *Prevalence of Chronic Kidney Insufficiency in the Communities of "La Isla" and "Candelaria", Chichigalpa*. Medical prevalence study. León, Nicaragua: Universidad Nacional Autónoma de Nicaragua.
Wu, Jindong, Dong Wang, and Marvin E. Bauer. 2007. "Assessing Broadband Vegetation Indices and QuickBird Data in Estimating Leaf Area Index of Corn and Potato Canopies." *Field Crops Research* 102 (1) (April): 33–42. doi:10.1016/j.fcr.2007.01.003.
Xavier, Alexandre Cândido, Bernardo F. T. Rudorff, Yosio Edemir Shimabukuro, Luciana Miura Sugawara Berka, and Mauricio Alves Moreira. 2006. "Multi-temporal Analysis of MODIS Data to Classify Sugarcane Crop." *International Journal of Remote Sensing* 27 (4): 755–768. doi:10.1080/01431160500296735.
Zakaluk, and R. Sri Ranjan. 2008. "Predicting the Leaf Water Potential of Potato Plants Using RGB Reflectance." *Canadian Biosystems Engineering* 50: 7.1–7.12.

Joint European Master in Environmental Studies (JEMES)

Chapter 3

Geometric Corrections of Multispectral Images of a Mountainous Area

Case Study: Bertolina Eddy Covariance Tower site in the Spanish Pyrenees

by
Inti Luna Avilés

Supervisors:
Jacob Keizer
Agustin Lobo Aleu

October, 2012

Abstract

The FLUXPYR project is an European cross-border network for the determination and management of water, carbon and energy fluxes and stocks in agricultural and grassland ecosystems of the Pyrenees, in the context of climate and land-use change. In this project, monitoring of vegetation is being carried by remote sensing in order to upscale information from the field. However, conventional satellite images are not sufficient to cope with the revisit rate and required resolution to understand certain vegetation processes. For this reason, a working group is focusing on the use of UAV and multispectral cameras that provide much richer spectral information than conventional cameras. In this study, Images acquired at different altitudes over the rugged terrain of Bertolina in the Spanish Pyrenees were used to evaluated standard procedures of geometric correction and alignment between bands. A necessary step for the comparison of images from different sensors, different dates and to relate images with existing geo-databases and field data. As result, the geometric error obtained from images acquired at different altitudes was similar in terms of meters and it as much larger in terms of pixels when images were acquired at lower altitude. In addition,despite having reduced the geometric error to ~ 2.5 pixels for the area of main interest for higher altitude images, the outcome was not satisfactory since an important part of the area covered by the images had a much larger error. Also, identifying and accurately positioning the GCP at this resolutions is laborious and very often not enough GCPs could be found. Therefore, other strategies should be explored to reduce the geometric error and to improve the efficiency concerning the total processed area and time invested for that purpose. One of the approaches to be explored is bundle block adjustment technology, which produces orthorectified georeferenced mosaics by means of the automatic generation of tie points among images and which is implemented in some commercial softwares such as ENSOMOSAIC.

Table of Contents

3.1 Introduction

The FLUXPYR project is an European cross-border network for the determination and management of water, carbon and energy fluxes and stocks in agricultural and grassland ecosystems of the Pyrenees, in the context of climate and land-use change. The project focuses on climate and land use change in the Pyrenees, whose ecosystems are known to be particularly fragile and impacted by global warming and changing hydrology. It involves multi-disciplinary teams from Spain, France and Andorra, and combines continuous flux and discrete stock assessments based on ecosystem, atmospheric and satellite studies. One of the main source of information comes from the use of micro-meteorological stations (Eddy Covariance Technique) located at different altitudes, along with remote sensing (e.g. satellite and aerial images) and modeling of different processes, to assess the impacts of climate and land use change in the Pyrenees, and to propose guidelines for sustainable land and resource management(“FLUXPYR” 2012)

In order to upscale results from the ground obtained with the Eddy Covariance Tower and vegetation classification on-site, satellites images are traditionally used. However there is a need for higher temporal and spatial resolution. In that sense, one working group of the project is evaluating the use of different sensors and platforms such as small planes and Unmanned Aerial Vehicles (UAV) in order to get higher spatial and temporal resolution. This information combined with Geographical Information Systems (GIS) allows the study and modeling of snow cover, land cover and use, carbon storage and vegetation dynamics.

In the previous chapter we have shown that while imagery acquired in the visible part of the electromagnetic spectrum is able to provide relevant information on

plant properties, multispectral imagery including NIR bands provides much richer information. For this reason, a multispectral camera is being used in FLUXPYR.

In the course of this project geometric correction is a required processing step which assigns proper planimetric map locations to individual picture elements (pixels). This step is necessary for the comparison of images from different sensors, different dates and to relate images with existing geo-databases(Kardoulas et al. 1996; Jensen et al. 2002; Santhosh and Renuka 2011).

The purpose of this chapter is to evaluate the application of standard empirical methods of geometric correction to images acquired with a multispectral sensor (MiniMCA) in the Bertolina Eddy Covariance study site.

3.2. Methodology

3.2.1 Sensor and Image Acquisition

Nowadays, an interesting sensor for vegetation studies is the MiniMCA multispectral camera (**Figure 3.1**) manufactured by Tetracam (www.tetracam.com) due to its relatively low cost, the independent sensors of each band and flexibility of changing the filters by the user which is very useful when investigating different vegetation types at different wavelengths of the electromagnetic spectrum. Using the technical characteristics (**table 3.1**) the mission was planned to acquire images at different altitudes in order to evaluate resolution and processing requirements with information from visible and near infrared part of the spectrum (**table 3.2**).

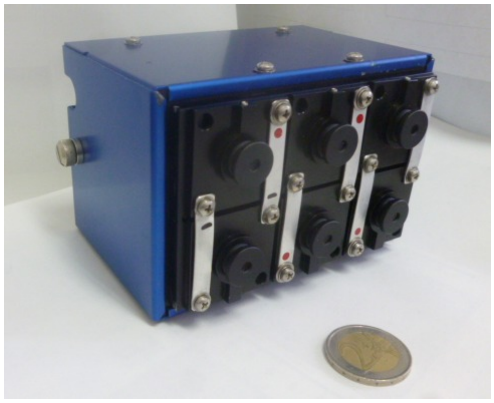

Figure 3.1. Mini MCA Camera

Table 3.1. Camera Technical Characteristics.

SXGA resolution	1280 x 1024
Megapixels	1.3
Focal distance (mm)	8.5
FOV format	4:3
Pixel size (μm)	5.2
Sensor dimensions (mm):	6.66 x 5.32
Filter diameter (mm)	25
Time required for single shot (s)	3-5
Camera Weight with filters (gr)	700
Energy requirements (voltage and current)	12-14VDC and 450 ma

Table 3.2. Filter configurations

MCA01			
Filter Code[1]	Spectral Region	Spectral Range (FWHM[2]) (nm)	Spectral Width (FWHM) (nm)
450FS20-25	blue	441.439 - 459.977	18.538
550FS10-25	green	546.519 - 556.409	9.890
670FS10-25	red	666.809 - 676.385	9.576
710FS10-25	NIR	706.841 - 716.454	9.613
730FS10-25	NIR	727.260 - 737.306	10.046
780FS10-25	NIR	777.904 - 787.333	9.429

1 Andover Corp. http://www.andovercorp.com/Web_store/Standard_BP/Std_BP_General.php
2 Full Width at Half Maximum ((Liang 2004))

The study site was located at Bertolina in the Spanish Pyrenees about 1200 m above sea level (**Figure 3.2**) where 82 images were acquired on June, 2012 (**table 3.3**) at 400 and 1100 m above ground level (AGL) covering an area around the Eddy Covariance tower.

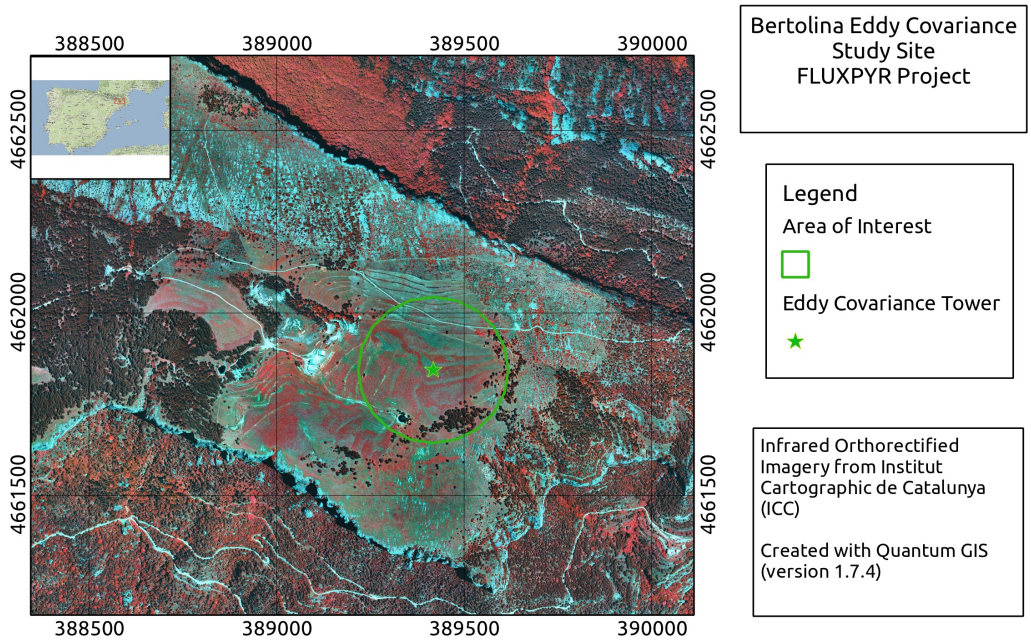

Figure 3.2. Location Map of Bertolina Eddy Covariance Tower, Spain

Table 3.3. General Characteristics for the flight.

Date	2012/06/21
Camera settings	Automatic exposure, 10 bits RAW
Average Height (AGL)	400 and 1100 m
Pixel size (m)	0.18 m (400m AGL) and 0.58m (1100m AGL)
Total images	82

3.2.2 Image Processing

Images files were acquired in proprietary RAW format and where transformed to multipage Tif file using PixelWrench2, a software from Tetracam company. Tetracam MiniMCA camera has 6 lens, and thus in order to have pixels from the 6 bands in the same location and alignment process is performed by PixelWrench2 using a calibration file specific for each camera.

These images can not be opened by GIS softwares as multi band images and required another transformation performed with a program function developed by Dr. Lobo using R software.

3.2.2.1 Geometric Correction

Georeferencing was performed using the Georeferencer Tool in QGIS. This procedure was performed twice for images acquired at an altitude of 1100 m and once for images acquired at 400 m (AGL). For images acquired at 1100 m of altitude, the first geometric correction was carried out using several control points distributed along the image and the second time was using only control points within the area of interest (AOI) near the eddy covariance tower applying a third degree polynomial transformation always with a nearest neighbor interpolation method. This transformation was applied because the terrain was of complex topography. Images acquired at 400 m of altitude were georeferenced using a first degree polynomial transformation because there were few reference feature that could be used as control points.

3.2.2.2 Alignment Evaluation

One difficulty when working with a camera with 6 lens is the alignment between the bands. For the MCA, this is carried out using an alignment file specific to each camera that contains information used by PW2 to register each slave camera image to the master camera image prior to writing them as a Multipage Tif from

the RAW images. This alignment file align all the bands with respect to a master band. However, alignment changes depending on the distance of the object in the image with respect to the camera. For this reason, while an image acquired at a certain height do not present visible misalignments, when the height is decreased, the misalignments increased which is a problem when it is required to extract information from a certain location, as the pixels from each band for the same feature have different locations. To evaluate the alignment error an feature on the image was selected and points where located on feature for each band. Later, distances between the points were measured and compared with the master band and between each other.

3.3. Results and Discussion

3.3. 1 Geometric Correction

Eight Images were selected for georeferencing at two different altitudes and with different exposure time(**table 3.4**). Pixel resolution of images at higher altitude was of 0.58 m and of 0.18 m for images acquired at lower altitude.

Table 3.4. Selected Images for Geometric Correction

Height (m AGL)	Exposure (ms)	File name
1136	2.70	1293
1085	2.75	1294
1123	2.20	1311
1099	1.65	1312
412	1.35	1359
404	1.30	1360
around 400*	1.30	1361
380	1.20	1362

*There was an error with camera-gps connection so the exact altitude for that image was missing.

The first geometric correction was carried out using control points on the whole area covered in the scene and the second one only using control points inside the main area of interest (AOI), where the tower is located (**Figure 3.3**).

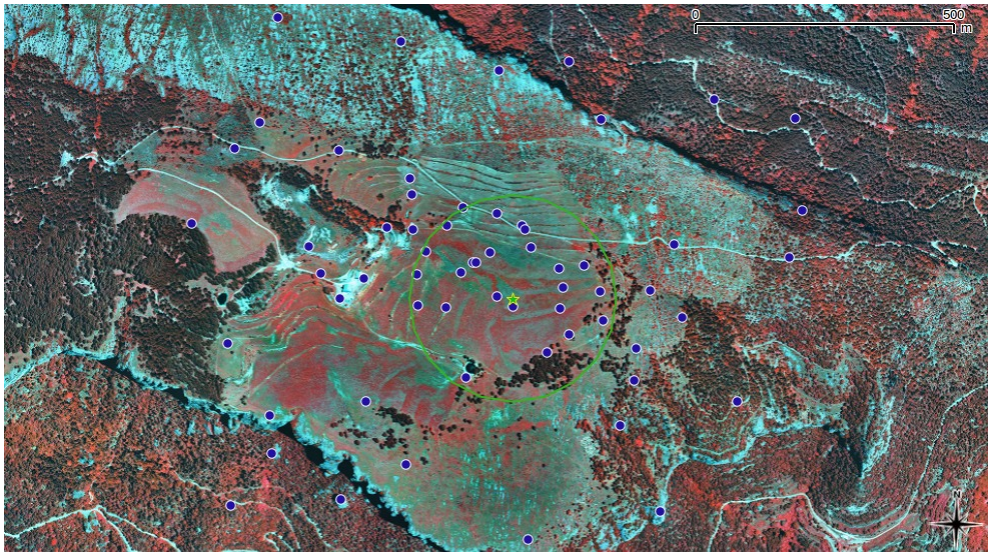

Figure 3.3: Ground control points used. Green circle represents the main area of interest and ground control points are displayed as blue dots.

Geometric Error for images acquired at 1100 m AGL

Geometric error from the first (whole scene) and second (AOI) geometric correction was compared and resulted in a lower mean error in the second geometric correction than in the first one (**table 3.5**). However, the geometric error for the second geometric correction at specific evaluation points was not always better than the first one (**Figure 3.4**). Comparing between images, the geometric error was larger in image 1294 and smaller in the image 1311. One possible reason for this was that the area covered by image 1294 had fewer clear features that could be used a control points compared to image 1311 that covered and area with many well defined features.

Table 3.5. Mean Geometric Error

Geometric Correction	Image 1293		Image 1294		Image 1311		Image 1312	
	m	pix	m	pix	m	pix	m	pix
1st Whole Scene	2.74	4.70	3.32	5.72	1.83	3.17	1.79	3.08
2nd Area of Interest	1.60	2.75	2.87	4.94	1.24	2.13	1.53	2.63

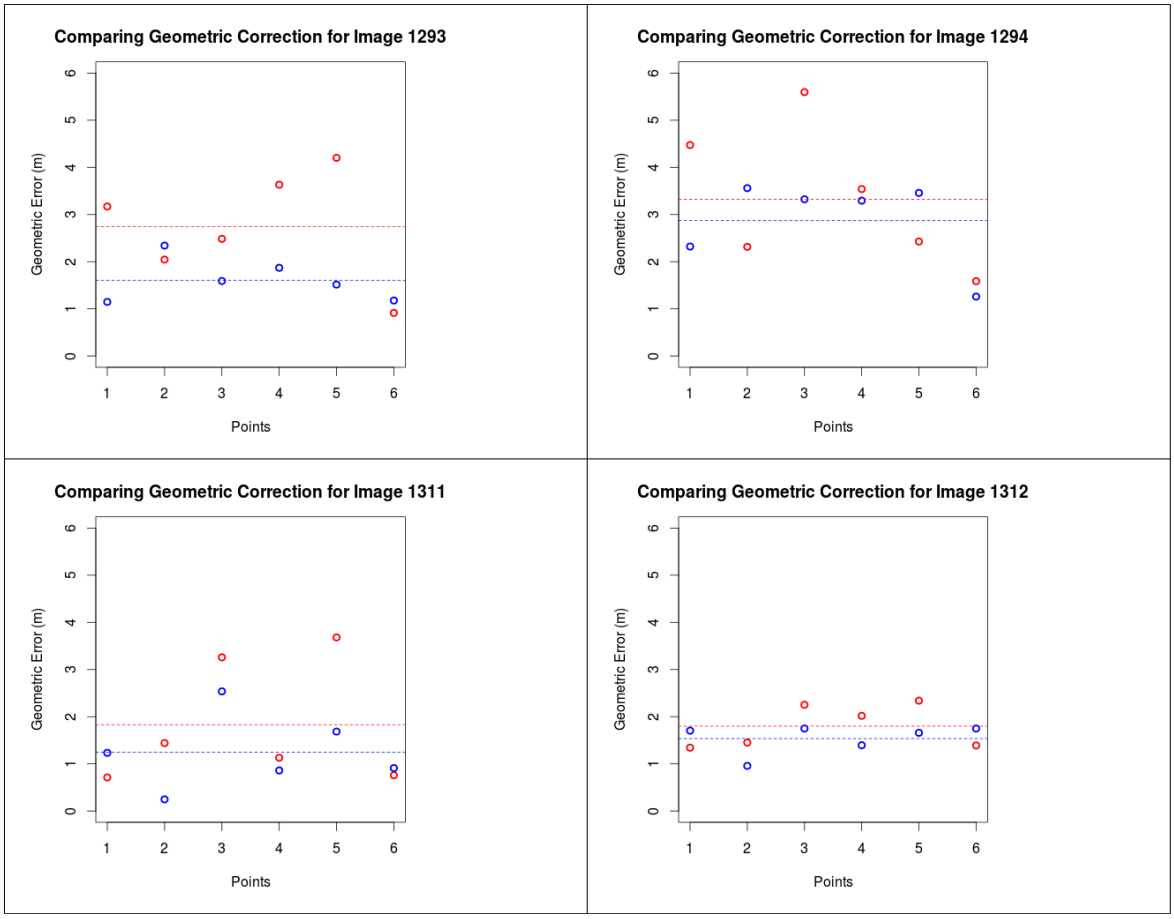

Figure 3.4. Geometric Error Comparison. Geometric error (m) for the first (red circles) and second (blue circles) geometric correction. Dot lines are mean values for each geometric correction.

Geometric Error for images acquired at 400 m (AGL)

As a consequence of having less area covered (**Figure 3.5**), fewer features could be used as ground control points (GCP) in the reference image which affected the geometric mean error. From the 4 images selected for geometric correction only two of them had enough ground control points for a first polynomial transformation, the other two had to be corrected taking as reference points features from the other two images already georeferenced. Thus evaluation was performed only on the images with enough GCP from the reference imagery.

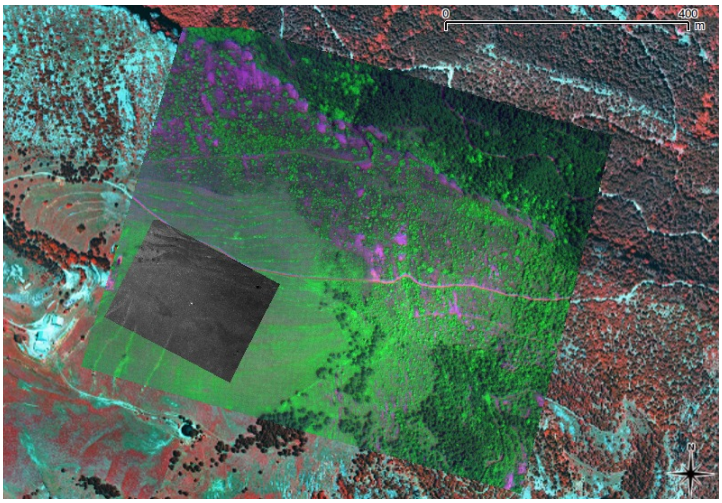

Figure 3.5. Comparison of area covered by images acquired at different altitudes. 400 m AGL (gray color) and at 1100 m AGL (green color).

The mean error of the two images evaluated is presented in **table 3.6.** Comparing to images acquired at 1100 m, this images presented a similar error in terms of meters but a much higher geometric error in pixels since the pixel size was smaller.

Table 3.6. Geometric error for images acquired at 400 m AGL

Geometric Correction	Image 1359		Image 1362	
	m	pix	m	pix
mean	1.49	8.29	1.95	10.82

3.3.3 Alignment Evaluation

The alignment between bands was evaluated using an image acquired at 400m AGL (image 1361) and an image at 1100 m AGL(image 1293). **Figure 3.6** represents the location of a reference point for each band on the reference pixel grid of the master band 6.

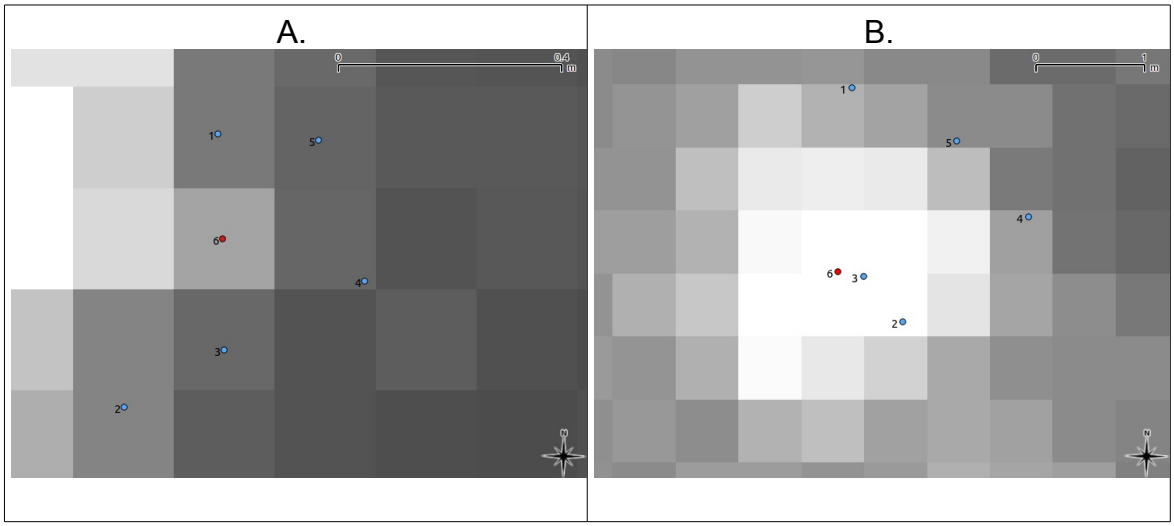

Figure 3.6. Alignment error evaluation. Points indicate the location of the same pixel in different bands. A. Image at 400m AGL. B. Image at 1100 m AGL. Master band (6) displayed in red and the rest in blue.

Comparison of each slave band with the master band (b6) was performed (**table 3.7**). For the image acquired at 400 m AGL, bands 1 had the smallest error of 1.05 pixels and band 2 presented the largest error of 1.94 pixels. For the image acquired at 1100 m, band 3 had the smaller error of 0.41 pixels, while bands 4 had the largest error of 3.13 pixels.

Table 3.7. Alignment error between slaves and master band (band 6).

Bands	Image 1361 (400 m AGL)		Image 1293 (1100 m AGL)	
	Distance (m)	Distance (pixels)	Distance (m)	Distance (pixels)
b1	0.19	1.05	1.69	2.91
b2	0.35	1.94	0.75	1.29
b3	0.20	1.11	0.24	0.41
b4	0.26	1.44	1.82	3.13
b5	0.25	1.39	1.62	2.79
Mean	0.25	1.39	1.22	2.11

From the operational point of view, the maximum alignment error between bands must be considered. In the image at 400m maximum alignment error was found between bands 2-5 (**table 3.8**) with a geometric error of 0.60 m (3.33 pixels) and in the image at 1100m the largest displacement was found for bands 1-2 with a geometric error of 2.19 m (3.78 pixels)

Table 3.8. Maximum error between bands

	Image 1361 (400 m AGL)	Image 1293 (1100 m AGL)
Bands	b2 - b5	b1 - b2
Distance (m)	0.60	2.19
Distance (pixels)	3.33	3.78

Comparing between images from different altitudes, the maximum alignment error in pixels is similar having 3.33 pixels for the image at 400m AGL and 3.78 pixels for the image at 1100m AGL. However, the difference is more important in meters having 0.60 m and 2.19 m respectively.

The discrepancy in the relative position of the reference pixel across bands between the image acquired at 400 m and 1100m AGL was not expected. One likely explanation is the change of roll and pitch angles of the plane at the moment of image acquisition, but further analysis should be performed to understand better the causes of the misalignments and how to properly align the bands.

3.4 Conclusions

Although images of low altitude (400m AGL) had higher resolution, they have a similar geometric error measured in meters and a much higher error in pixels compared to images acquired at 1100m AGL. Therefore, low altitude images processed with the georeferencing method described in this study present disadvantages because they required an equal effort to georeference a much smaller area and with a higher geometric error measured in pixels.

Taking into account the geometrical error of the images that were around ~ 2.5 pixels (images acquired at 1100m AGL) for the area evaluated and the maximum alignment error of 3.7 pixels, it should be account for a total error of 6.2 pixels error. In addition, taking into account that the geometric error should be around 20% of the size of the object of study and the size of the pixels in this case is of 0.58 m, then the minimum unit of comparison should be ~ 28 pixels which is equivalents to ~15 m.

Despite having reduced the geometric error to ~ 2.5 pixels for the area of main interest, the outcome was not satisfactory since an important part of the area covered by the images had a much larger error. Also, identifying and accurately positioning the GCP at this resolutions is laborious and very often not enough GCPs could be found. Therefore, other strategies should be explored to reduce the geometric error and to improve the efficiency concerning the total processed area and time invested for that purpose. One of the approaches to be explored is bundle block adjustment technology, which produces orthorectified georeferenced mosaics by means of the automatic generation of tie points among images and which is implemented in some commercial softwares such as ENSOMOSAIC (Pellikka et al. 2009).

3.5 References

"FLUXPYR." 2012. Accessed October 10. http://www.fluxpyr.eu.

Jensen, J.R., Botchway, K., Brennan-Galvin, E., Johannsen, C., Juma, C., Mabogunje, A., Miller, R., et al. 2002. *Down to Earth: Geographical Information for Sustainable Development in Africa*. Washington: National Research Council. http://www.nap.edu/openbook.php?isbn=0309084784.

Kardoulas, N. G., A. C. Bird, and A. I. Lawan. 1996. "Geometric Correction of SPOT and Landsat Imagery: A Comparison of Map-and GPS-derived Control Points." *Photogrammetric Engineering and Remote Sensing* 62 (10): 1173–1177.

Liang, Shunlin. 2004. *Quantitative Remote Sensing of Land Surfaces*. Wiley-Interscience.

Pellikka, Petri K.E., Milla Lötjönen, Mika Siljander, and Luc Lens. 2009. "Airborne Remote Sensing of Spatiotemporal Change (1955–2004) in Indigenous and Exotic Forest Cover in the Taita Hills, Kenya." *International Journal of Applied Earth Observation and Geoinformation* 11 (4) (August): 221–232. doi:10.1016/j.jag.2009.02.002.

Santhosh, B. D. S., and D. M. Renuka. 2011. "Geometric Correction in Recent High Resolution Satellite Imagery: A Case Study in Coimbatore, Tamil Nadu." *International Journal of Computer Applications* 14 (1): 32–37.

Tetracam Co. 2012. "How to Generate an MCA Alignment File". Tetracam Company.

Joint European Master in Environmental Studies (JEMES)

Chapter 4

Mosaicking and Geometric correction of UAV imagery using ENSOMOSAIC

A case study: Montseny Natural Park

by

Inti Luna Avilés

Supervisors:

Jacob Keizer

Agustin Lobo Aleu

October, 2012

Abstract

The Natural Park Montseny is under constant change, reason for which is being monitored using remote sensing to evaluate the changes in vegetation, monitor areas under anthropogenic pressure and possibly locate invasive species. All these aspects could be explored in a cost-effective way once proper geometric correction has been performed. This chapter focused on the geometric correction processing using bundle block adjustment technology and automatic tie point detection between images using an available commercial software such as ENSOMOSAIC in order to produce orthorectified and georeferenced mosaics. In addition, time required was recorded and the geometric error of the products was evaluated by comparing them to the official orthorectified imagery. Images were acquired during two flights in two different areas of the park. The first flight was not planned according to software requirements and as consequence there was not enough overlap between images producing a severe mean errors of ~20 m. While for the second flight overlap requirements were considered producing a mosaic with higher geometric quality with a mean error of 2.3 m. Required time per mosaic was around 40 hours, more time than expected and it was probably due to the lack of inertial movement angles information during flight which did not allow to use automatic linking and accurate point generation. Despite UAV are able to acquired high resolution imagery, their use and their cost are dependent of orthorectification processing and are especially important when it is intended to compare imagery with other geo-data in areas with high relief.

Table of Contents

4.1 Introduction

El Montseny Natural Park is located in the Catalan pre-coastal mountain range, of which this massifconstitutes the area with highest altitude. It covers an area of 31,063.94 hectares, spread over eighteen municipalities in three regions (Osona, La Selva and El Vallès Oriental). The relief of El Montseny starts with elevations of under 200 m on the eastern side that rise to over 1,700 m.

The broken mosaic formed by the diverse terrain gives the Natural Park its climatic diversity (differences in humidity and temperature), variety of habitats, biological wealth of mountain ranges, streams, woods, cropland and high plains. This climatic diversity comes with different types of vegetation. In the form of zones, and as the altitude rises, the characteristic Mediterranean plant formations are found in the lower parts, rainy middle mountain types higher up, Central European environment at over 1,000 m, and finally sub-alpine habitat at the summit. Therefore, Montseny Natural Park has high ecological value and features the presence of some remarkable examples of endemism. In addition, the presence of man in the area from remote times has modeled a humanized landscape emphasizing even more the partitioning of the ecosystem. Due to its importance, UNESCO included El Montseny in the MAB (Man and Biosphere) World Network of Biosphere Reserves in 1978.

The Special Plan for the Protection of the Natural Environment and Landscape of El Montseny Natural Park became effective on 31 January 2009. The plan is intended to provide a tool to make El Montseny a vital, dynamic region, where protection of the natural environment is compatible with the life quality of the people who live there and the enjoyment of visitors. This plan proposes the monitoring of the area given the threats and different problems affecting the Natural Park such as the water scarcity for human activities, forest changes including invasive species, uncontrolled tourism in certain areas, forest fires, climatic changes affecting the natural habitats, the species and the agriculture *(Boada et al. 2010)*.

Certain aspects of the monitoring plan could be carried out using remote sensing, but the traditional platforms for that such as satellites and aircrafts present certain limitations such as the high cost, weather dependency, and the spatial and temporal resolution might not be sufficient.

One alternative is the use of low-altitude remote sensing (LARS) systems as the ones operated with unmanned aerial vehicles (UAV) which were originally created for the military sector and have recently been used for civil applications such as agriculture and forest monitoring in different parts of the world (Swain et al. 2007)

However, the UAV platforms are generally more unstable than traditional aircrafts and the processing of their imagery could be time consuming and represent a limitation for its use, especially when it is required to cover the same area many times, and thus pixels´ geolocation should match as much as possible along different aerial surveys.

As part of the solutions recently created to increase the processing speed of imagery and the accuracy of the mosaics created, certain technology based on bundle block adjustment and light propagation, is being used to created mosaics from small format imagery that is orthorectified and could also be used to create digital elevation models (DEM). Such technology is being used for monitoring forests, rodes, watersheads and changes in land use among many other applications ((Pellikka et al. 2009)

The purpose of this study was to describe the use of ENSOMOSAIC for creating orthorectified mosaics using UAS imagery of Montseny Natural Park and evaluate the geometric error using reference imagery.

4.2 Methodology

4.2.1 Study Area

The imagery was acquired on two dates and in two different locations in Montseny Natural Park (**table 4.1** and **Figure 4.1**). For this purpose a small UAV operated from a ground station was used, carrying as payload a SIGMA DP1 camera with a FOVEON sensor and a modified filter configuration , allowing the NIR part of the spectrum to pass and blocking the blue band, using a yellow filter.

Table 4.1. Flight missions information

Information	Flight 1	Flight 2
Date	November 5, 2009	February 16, 2010
Location	Aiguafreda	Pla de la Calma
Coordinates	440060 E, 4628001 N	443674 E, 4623111 N

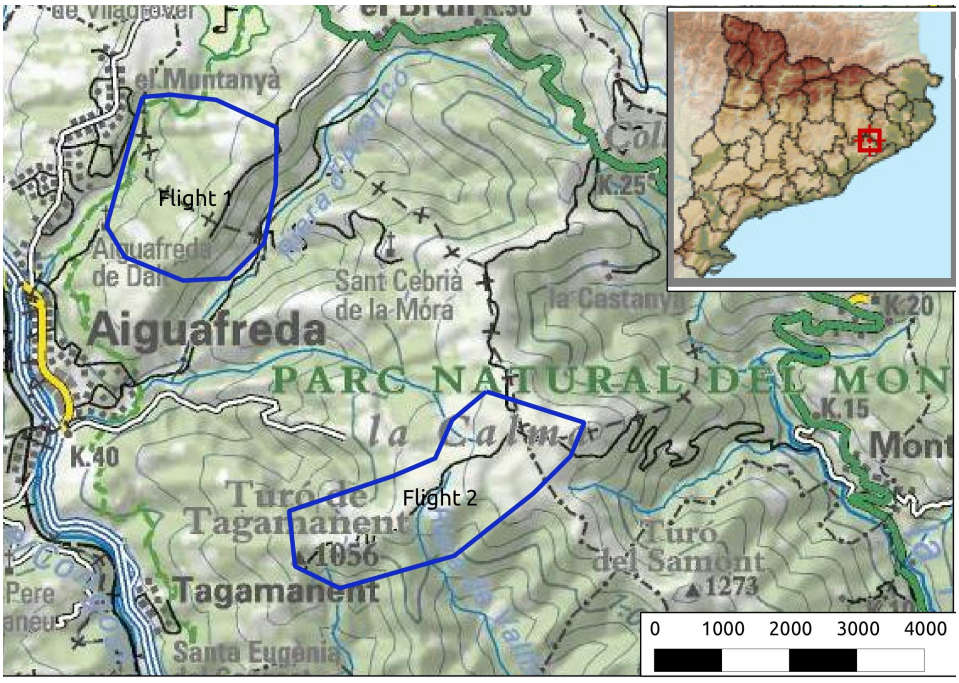

Figure 4.1. Location map of the study area

4.2.2 Sensor

The mission was planned using specific functions created by Dr. Agustin Lobo for R and QGIS,while knowing the area to be covered, the desired resolution and the camera parameters for the Sigma DP1 (**table 4.2**).

Table 4.2. Camera Technical parameters

Parameter	Value
Focal length	16.6 mm
Sensor size	20.328 x 13.552 mm
Pixel size	0.0077 mm
Image dimension	2640 x 1760 pixels
Image format	Proprietary SIGMA RAW

4.2.3 Unmanned Aerial Vehicle (UAV)

ATMOS UAV is a series of versatile, medium-range and low-cost mini-UAV (**Figure 4.2**) propelled by a silent electric engine, able to carry a payload of up to 330 g (total weight of the platform: 1.8 kg), remotely-controlled from a control cabin within a radius of 15 km and with 2 h of flight autonomy. Conventional (non-geodetic grade) GPS data are transmitted in real-time to the control cabin, from which both navigation and image acquisition are controlled(Lobo 2009).

Figure 4.2. ATMOS-3 Platform. Image taken from Lobo (2009).

4.2.4 Image Processing and Mosaicking

Orthorectification and mosaicking was performed with the ENSOMOSAIC software (v. 7.3). ENSOMOSAIC is a digital aerial imaging and image processing system developed by MosaicMill Oy and its partner companies. The software uses bundle block adjustment technology (BBA), as well as tie and ground control points that can be created automatically and manually, depending on the data (and its quality) recorded during the flight, in order to produce an orthorectified mosaic. This BBA is based on a mathematical model that assumes that the behavior of the ray of light passing through the optics of the camera is known. Therefore, the optical characteristics of the camera (focal distance, principal point of the camera, and distortion of the sensor-lens) must be known with high accuracy *("EnsoMOSAIC Image Processing User's guide v.7.3" 2009)*.

Calibration of the camera optics was carried out by taking pictures of a target (supplied by ENSOMOSAIC co.) from different positions while distances, angles and target dimensions were known . The resulting images were sent to the company in order to produce a camera calibration file using the calibration software RapidCal (*http://www.pieneering.fi/*) that is sold separately. The calibration file contains all geometric parameters required by ENSOMOSAIC.

ENSOMOSAIC requires the data from the flight to be in specific formats, thus several files are required as input for the processing. Such files and the data contained in each type are:

name.TRP

Project file, the images´ID, the specific directories for images, GPS data, average terrain altitude

name.GPS

It contains the GPS information for each image used as input for mosaicking.

Name.CAL

Camera parameters obtained from target image processing.

Images .

Folder with images.

Name.GCP

Ground control points. This is a optional file and it contains specific coordinates and height (x,y,z) for known locations in the input images. In addition, deviations of the coordinates are established for adjusting the BBA.

Parts of the file can be seen in Appendix . These files were created according to the specific ENSOMOSAIC requirements using tailor functions in software R.

The general workflow for Ensomosaic is shown in **Figure 4.3** and it can be seen that depending on the type and quality of the data used for input (GPS precision, flight sensors used and flight stability), the procedures,processing time and quality of the output will vary significantly.

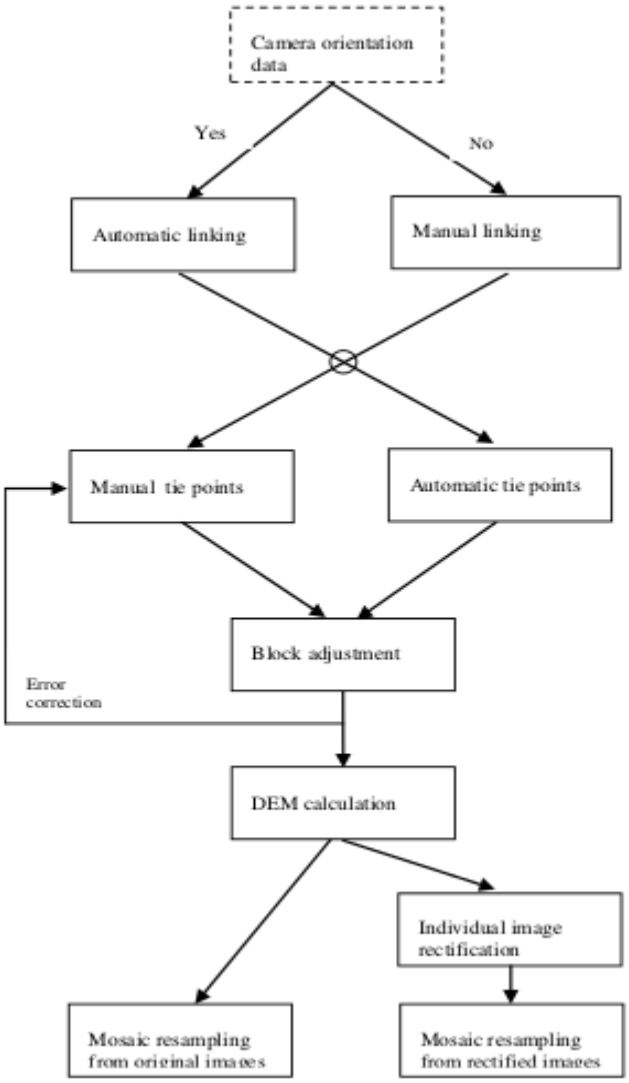

Figure 4.3. Workflow for Ensomosaic mosaicking procedure[1].

The specific procedures and the required time for this study are presented below:

Images were tiled for fast display during the visual inspection.

Images were linked manually since there was no camera orientation information (yaw, pitch and roll of the platform). Images Linking was carried out by selecting three common points between each pair of images forming a triangle where the points in the image should be as far as possible from each other. Linking is used to give a rough orientation of the images, an automatic step when IMU information is recorded.

1.Image taken from ENSOMOSAIC User guide (v.7.3)

Manual tie points were introduced to connect the images. Images should have at least 3 common points in each image quarter. The connection between images can be classified into 4 statuses depending on the number of tie points for each image quarter. (**table 4.3**). Thus, an image could have four quarters with different connectivity status (red,yellow,blue and green).

Table 4.3. Connectivity Color Code between images

Color Code	Number of points per image quarter
Red	0
Yellow	1-3
Blue	4-6
Green	7 or more

Ground control points were specified within the images.

Ground control points were identified and a vector point was generated for each location using the official 1:5000 infrared orthoimagery of 2009 and the official Digital Elevation Model (DEM) with a resolution of 10 m(*Instituto Cartografico de Catalunya* (ICC)) for the area.

Points (manual and automatic tie points and ground control points) are recorded as number of observation points which represent the number of times each point is present in all the images. For instance, 3 tie points (manual or automatic) could be present each in 5 images, counting for 15 observation points.

Aerial triangulation was applied.

Automatic Aerial Triangulation (AAT) window (**Figure 4.4**) was divided into 4 areas for locating tie points, bundle block adjustment processing, visualizing images to be used for the processing, and processing log (displaying the status of the processing and possible problems).

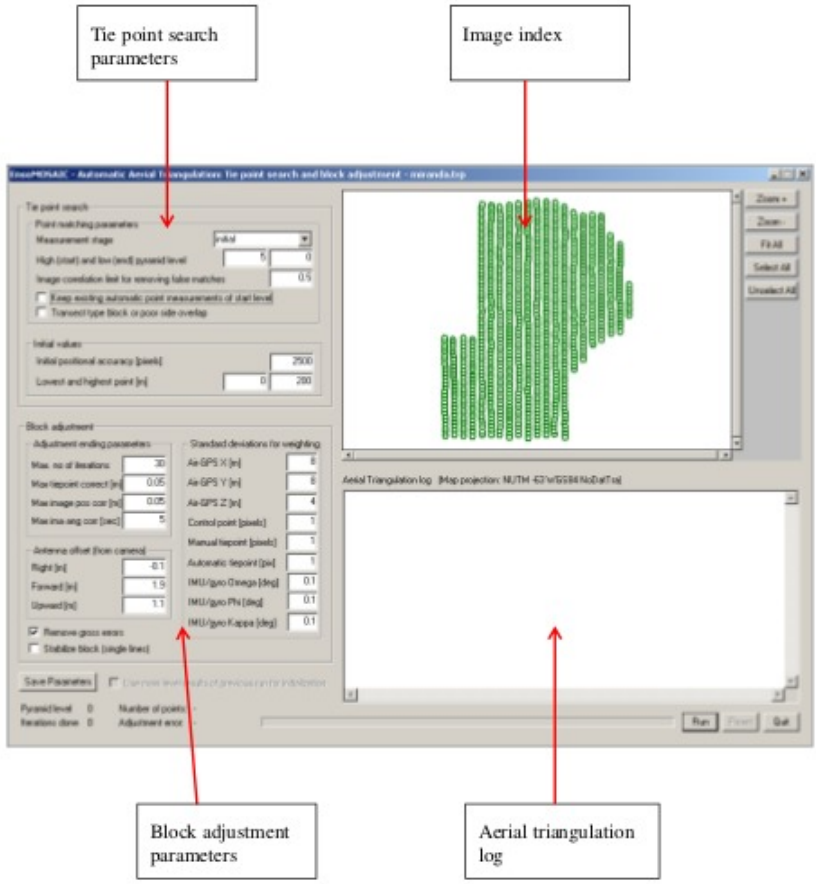

Figure 4.4 Automatic Aerial Triangulation (ATA) window.[2]

The AAT is carried out at different levels, working from the coarse image to the original resolution. The number of levels (pyramid level) depends on the size of the images and resolution and in order to get original resolution (level 0), upper levels have to be processed before (levels 5,4,3,2 and 1). For the images processed in this study the initial level was level 5 and the final level 0 (original resolution). However it is possible to create orthorectified mosaics at any level.

Tie point search parameters specify the region in which automatic tie points will be searched and the image correlation limit for removing false matches. The user enters the maximum distance allowed for tie point search and the image correlation limit, more correlation means more accurate point location but could

2 Image taken from ENSOMOSAIC manual v.7.3

be an insufficient number of points, so a lower correlation limit will be needed which produces more points (accurate and inaccurate). Thus, a balance should be found between number of points and accuracy of the location.

Bundle block adjustment parameters set the limits and requirements for the model to run and converge. These parameters can be classified in ending parameters, antenna offset, standard deviations for weighting and other considerations. Ending parameters specify the maximum number of iterations running the mathematical model, the stopping criteria for image correction in length and angles for image orientation correction. Antenna offset is the offset in x,y and z of the antenna in relation to the camera. Standard deviations determine the precision of the points (tie and ground control points) and gps, these parameters need to be adjusted for each flight and will vary depending on the quality of the information and the precision of the points used.

Other considerations are removal of gross errors, block stabilization used when there is low overlap or single line flights (used in this study) and additional image deformations which should be used when the camera is unstable, meaning that it has errors produced when it is without fixed focal length lens or the calibration information is inaccurate.

When running AAT, new automatic points are generated and a BBA is changed giving a BBA Adjustment Error which is the mean error of unit weight, a function of all the residuals and all the weights (deviations). However, other parameters should be verified in order to estimate the quality of the results such as the residual errors for points.

Residual errors for points were revised and high residuals were removed by verifying the correct position of each point in different images.

Bundle block adjustment was applied after each edition of points and step 5 was repeated until the error for the model was considered acceptable or until there was no further improvement to be made. BBA can also be applied using the BBA window where no point search is done and only the BBA parameters can be set.

Elevation Model

DEM was created using a 10meter cell resolution.

Mosaic Resampling

Mosaicking using the images and DEM previously created (**Figure 4.5**).

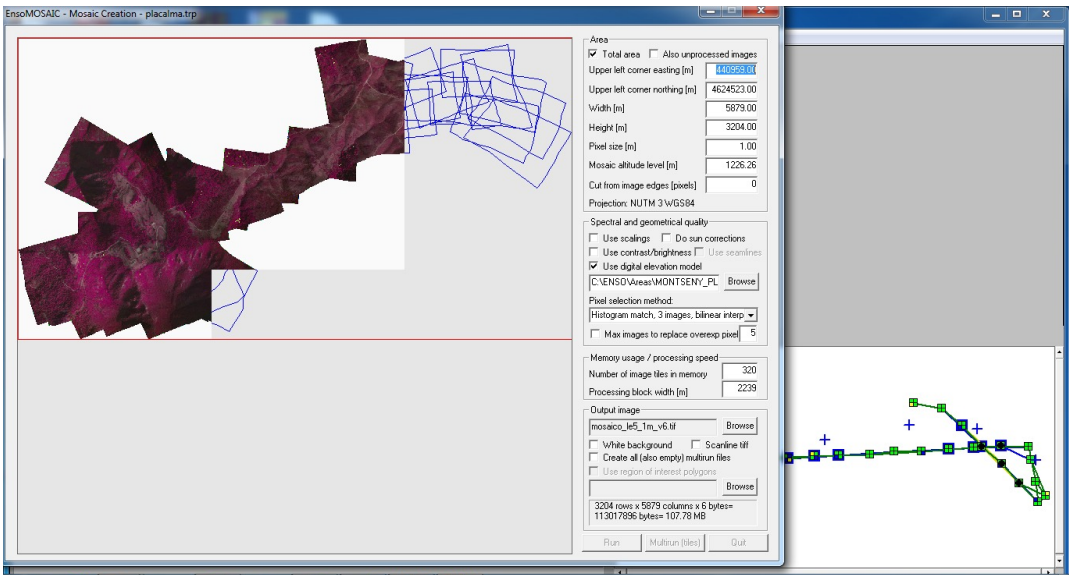

Figure 4.5. Mosaic Creation Window[3].

The mosaic was visually inspected comparing it to the official orthoimagery, if necessary tie and control points were modified and step 7-9 were repeated.

Geometric error estimation was carried out inside the convex hull of the mosaic. The convex hull is defined as the smallest polygon vector including all the points, which in this case were the ones used for orthorectification and mosaicking. Common points between the created mosaic and the official imagery were identified. These points were later used in R to calculate the euclidean distance between each point from the two sets of imagery using a custom function created by Dr. Agustin Lobo where two sets of georeferenced vector points were used as input and the pixel resolution was established, producing a table with the distance in meters and pixels.

3. Image taken from ENSOMOSAIC during Mosaic F2A3 creation.

4.3 Results and Discussion

4.3.1 Flight characteristics and Processing Parameters

The general characteristics of the areas and the mosaic processing applied is presented in **table 4.4.** The first flight was unstable. As a consequence, only 56% (13/23) of the images were accepted by ENSOMOSAIC given the pronounced angles at which they were acquired. In contrast, all (34/34) images from the second flight were accepted which is an indicator of the overlap between images and the stability of the flight.

Table 4.4. General characteristic for each flight

General Characteristic	**Flight 1**		**Flight 2**
Approximate Terrain Altitude (m)	1490		1100
Images taken	23		34
Images used	13		34
Area covered (sqkm)	2.0	1.08	7.15
Mosaics created	2		1

The ulterior use of ENSOMOSAIC had not been planned. Thus, the images did not have enough overlap. Also, since the platform was not carrying an inertial movement unit (IMU)to record pitch, yaw and roll angles (**Figure 4.6**), the processing of Ensomosaic had to be done with a large number of manual processes (linking between images, manual tie points and control points). Automatic tie points often were not accurate, which increased the processing time by visual inspection at each point in each image and adjusting its location.

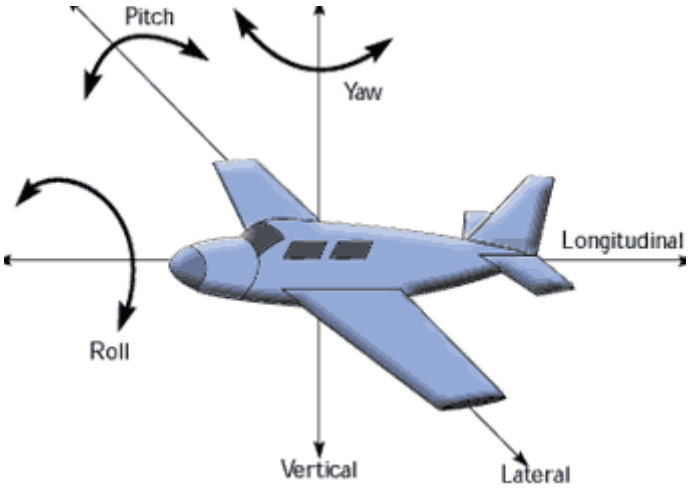

- **Figure 4.6.** Plane displaying pitch, roll and yaw movement[4] *(3axis Image* 2012)

The processing time was recorded for each area and is presented in **table 4.5**. the long time required for processing can be noted, which is not necessarily related to the total area covered by each mosaic only, but in this case, it is due to the overlap between images and the improvement of the geometric adjustment. It is important to keep in mind that this type of work cannot be done by the operator over large periods of time: the concentration required and the eyes capacity to focus on specific features decrease with fatigue, especially when there are homogeneous areas in the images.

Table 4.5 .Processing time requirements

	Mosaic 1 (F1A1)	**Mosaic 2 (F1A2)**	**Mosaic 3 (F2V1)**
Total time required	45-50 hours	35 hours	45-50 hours

Table 4.6 records the main parameters used for automatic point search options, as well as the number of image observation points and the standard error of the BBA which is a global indicator of the quality of the mosaic where a smaller value means a better geometrical quality.

These parameters where obtained with trial and error until the improvement made

4 .Image taken from NASA Aeronautics website: http://quest.arc.nasa.gov/aero/virtual/demo/aeronautics/tutorial/motion.html

was small compared to the time spent on it.

It can be seen that for the first flight, the angles used reach until 12 sec which for the second flight they were at 7 sec, an indicator for the stability of the flight. In the same manner, the correlation limit for point search was lower in the first flight than in the second one, which had an effect on both the amount and the quality of automatic points. It is important to note that a lower correlation between images around the points implies automatic location of more points. However, the error rate of these automatic points varies, so care should be taken in order to avoid the verification of large amounts of useless points.

It was learned that using more control points does not necessarily produce better results, while it makes it difficult for the software to converge to an acceptable solution, as it can be seen in **table 4.6**, the number of control points used and the adjustment error of the BBA do not correlate.

Table 4.6. Main parameters used and output quality characteristic for each mosaic

Mosaic	Correlation Limit for Point Search	Max. Angle Correction for BBA (secs)	Number of Image Observation Points			Adjustment Error BBA (pixels)
			Manual ties Points	Automatic ties Points	Ground Control Points	
F1A1	0.60	12	362	598	26	10.35
F1A2	0.70	5	216	1930	122	17.68
F2A3	0.85	7	1618	17556	7	0.78

4.3.2 Evaluation of Geometric Error

Resulting images of the mosaic of the first and second flight and the evaluation points used for estimating the geometrical error are displayed in **Figure 4.7.**

Image 1 F1A1 Flight 1 Mosaic 1 Scale 1:20.000	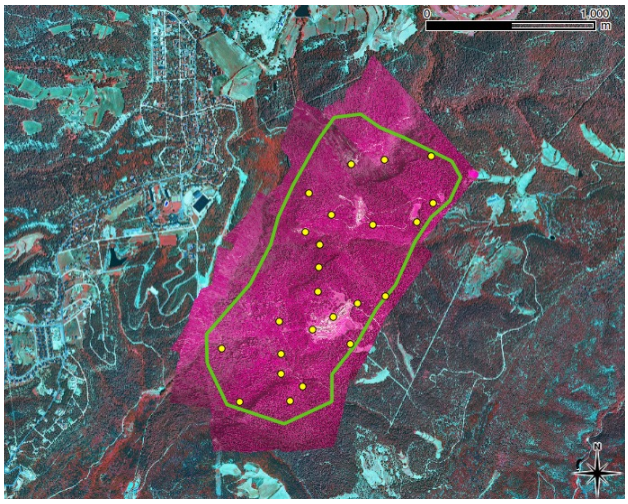
Image 2 F1A2 Flight 1 Mosaic 2 Scale 1:20.000	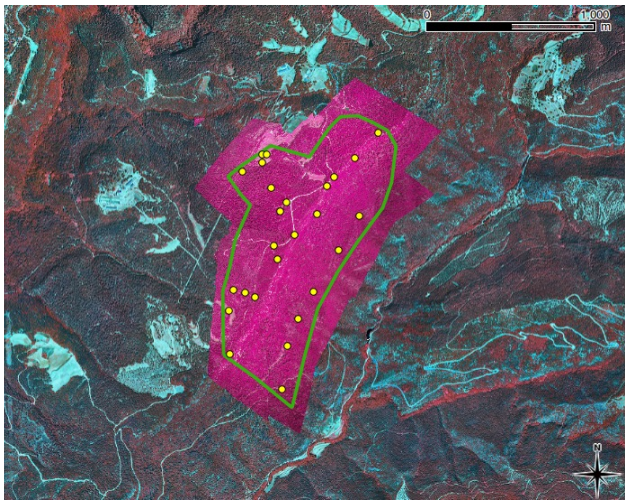
Image 1 F2A3 Flight 2 Mosaic 3 Scale 1:25.000	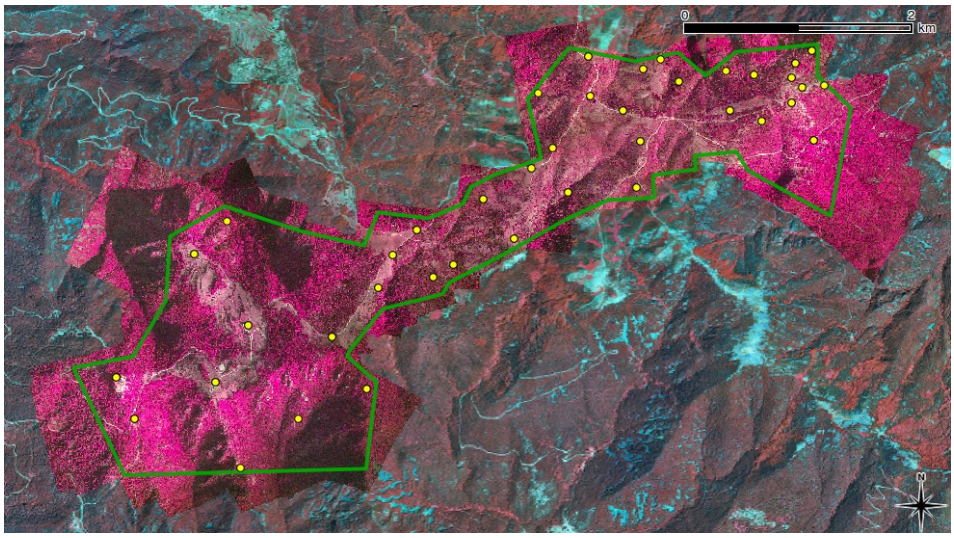

Figure 4.7. Evaluation points in yellow distributed along the mosaics.

The geometric error at the evaluation sites was measured as the euclidean

distance between the UTM coordinates in the mosaic and those of the official orthoimagery.

These errors were proportionally represented by the color and size of circles centered at the evaluation sites. The scale of the circles was created by dividing the geometric error in meters by 10 and color was ordered from light to dark blue (**Figure 4.8**) in QGIS for display.

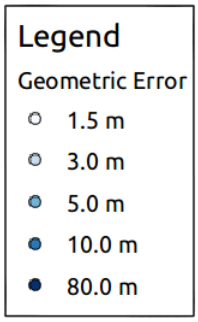

Figure 4. 8. Color code and range for error in meters

The geometric error for each evaluation site is shown in **Figure 4.9** for each mosaic. As expected, the error at the edges of the mosaics are greater than in the rest of the mosaicked area since there is not enough information from the bundle block adjustment model to reconstruct an accurate pixel geolocation. The green line represents the convex hull where the evaluation of the geometric error was carried out. Since some locations have a very small error compared to other areas, a yellow point was used as background to facilitate the visualization of the evaluation site. The error representation is on top of the white points, thus when the error is large enough, no white points are shown.

It is also important to note that when the border area is different in altitude than the rest of the area, the errors are even greater and this effect should be taken into consideration when planning missions with this type of platforms and using a similar software for image processing. One interesting option that the software presents is the option of selecting the area to be processed and using this option one could avoid using the borders of the mosaic where it is known that the error are greater.

Image 1 F1A1 Flight 1 Mosaic 1 Scale 1:20.000	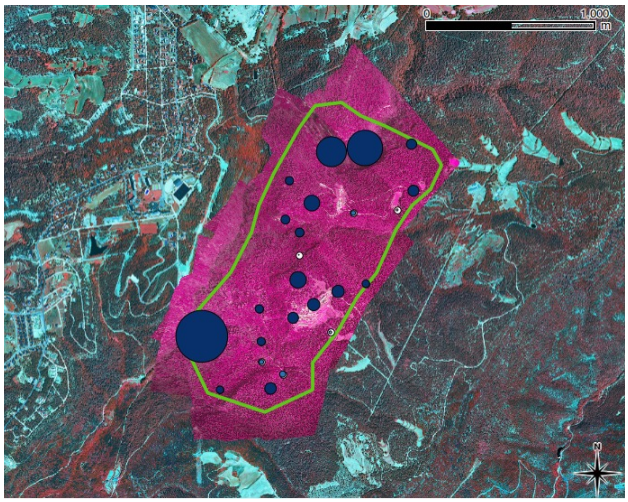
Image 2 F1A2 Flight 1 Mosaic 2 Scale 1:20.000	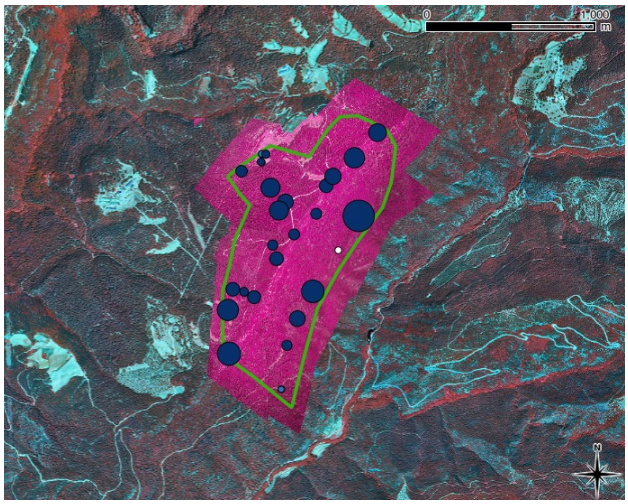
Image 1 F2A3 Flight 2 Mosaic 3 Scale 1:25.000	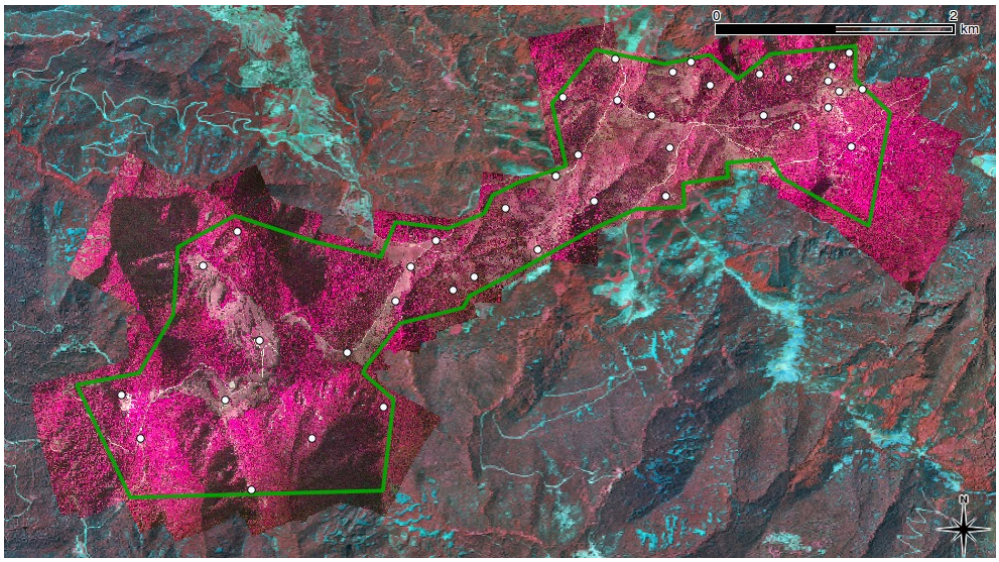

Figure 4.9. Geometric errors for each mosaic at evaluation points.

The interactive visual inspection of the three mosaics indicates that the third mosaic is of higher geometric quality. The differences and distribution of the errors are shown in the histograms for each mosaic (**Figure 4.10**) where he red vertical line represents the mean value.

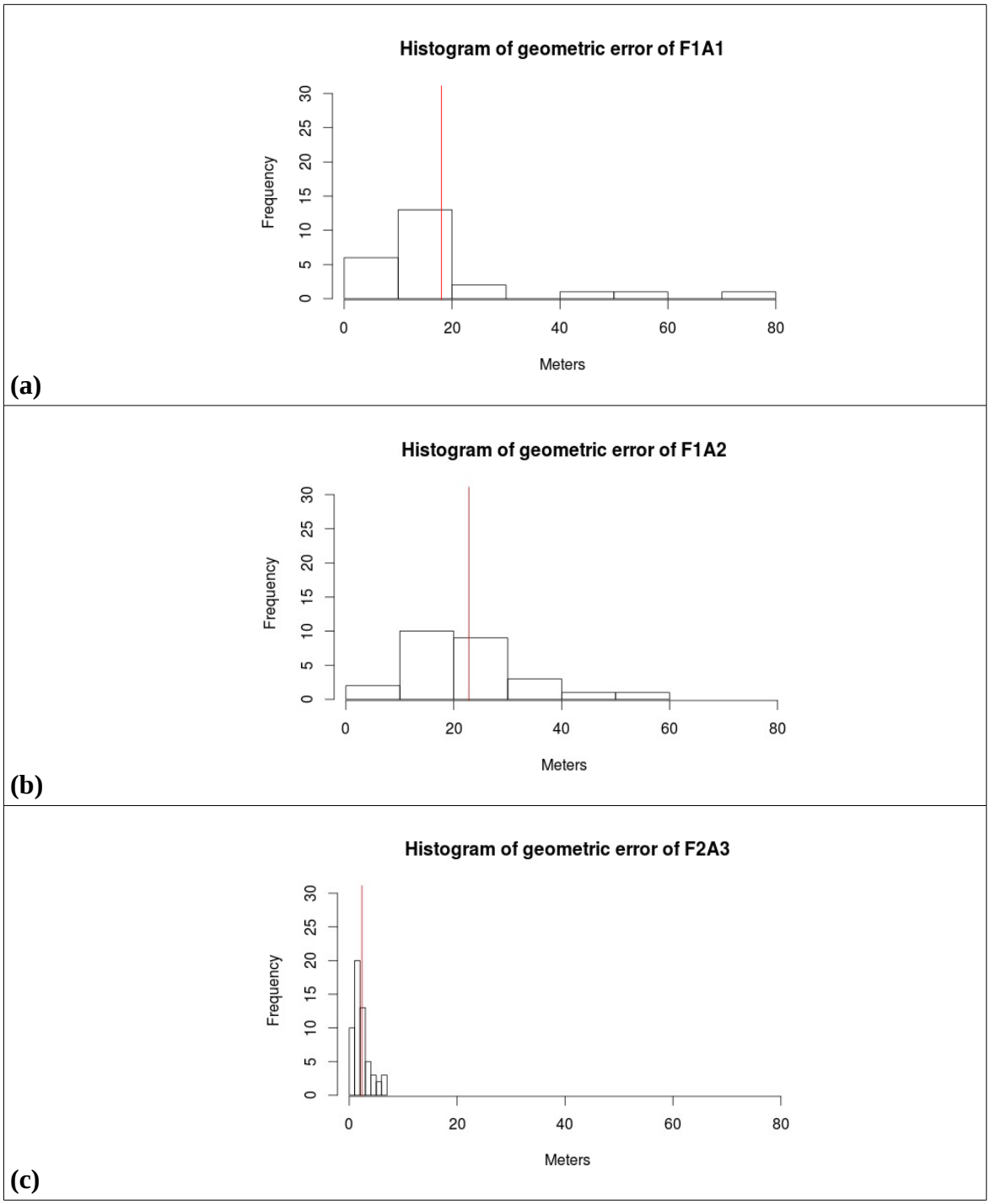

Figure 4.10. Histograms of geometric errors for each mosaic.

It was noticed that when a good adjustment error was obtained (i.e for mosaic F2A3 in first level of processing (level 5), a BBA adjustment error of 0.78 pixel was obtained), the subsequent levels went smoothly without no further manual intervention. However, the adjustment error alone is not the best indicator for the quality of the mosaic, and before moving to further levels of processing (4 to 0 in this mosaic), residual errors of points should be verified and a mosaic from the first level should be created and evaluated by visual inspection. Correcting erroneously located automatic and manual tie points could significantly improve areas where major deformations exist. Such errors occur especially after long hours looking of searching for tie points in homogeneous areas of the image.

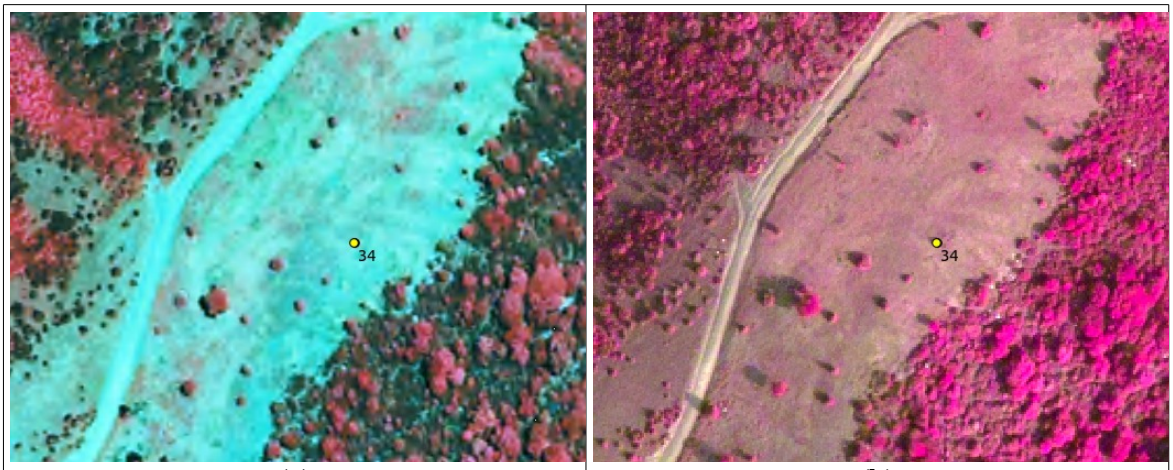

(a) (b)

Figure 4.11. Scene zoom on an area with 0.3m of geometric error (point 34). Point 34 in yellow (a) official orthorectified image and (b)mosaic F2A3.

While mosaic 3 (F2A3) was generally of high geometric quality (**Figure 4.8**), the borders of the mosaic present large errors especially when there is an abrupt change of altitude as presented in **Figure 4.9.**

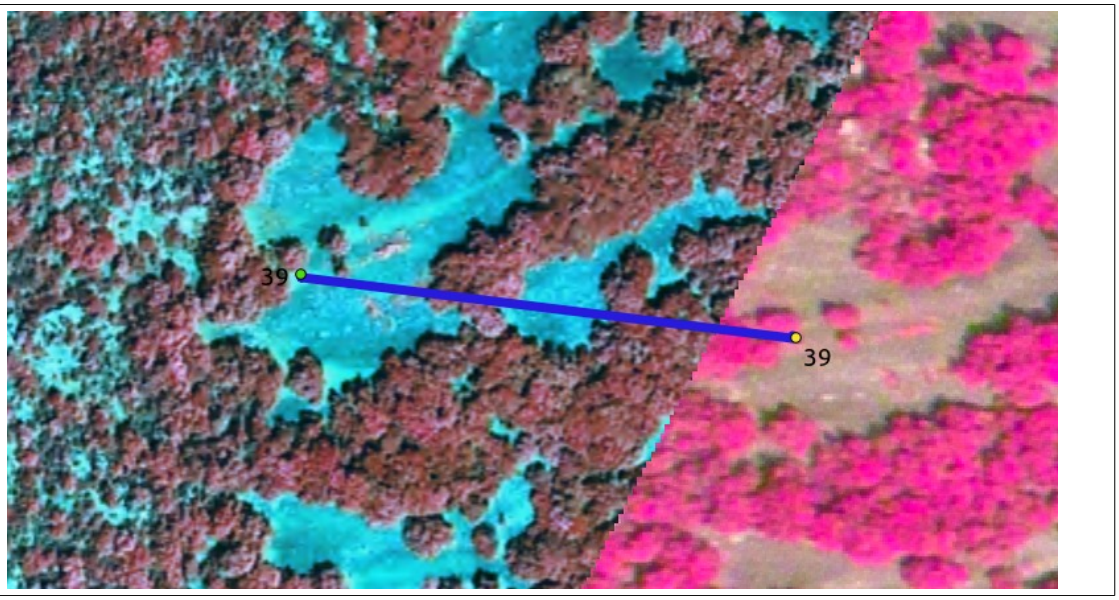

Figure 4.12. Scene zoom on an area with large geometric error for mosaic F2A3. Evaluation point 39 displayed in green and yellow. The geometric error is represented as a blue line of 107 m.

The geometric correction is of major importance whenever the image is to be compared with existing maps or with other images which is one of the purposes of using the UAV in the natural park, comparing changes of vegetation over time with high resolution imagery. Considering that the geometric error should be around 20% the size of the object of study, the mean of the geometric errors for each mosaic (**table 4.7**) indicates the limits of use. For that purpose the geometric correction should be improved and the processing should be sped up, perhaps by using an IMU unit recording the angles of the plane, using more than one flight line and increasing overlap between scenes, so a more stable bundle block can be generated. In our case only with mosaic 3 (F2A3), a mean error of 2.3 meters was reached which represents around four pixels.

Table 4.7. Geometric errors statistics for each mosaic

Mosaic	Mean error (meters)	Median Absolute deviation (meters)
F1A1	18.0	6.5
F1A2	22.8	10.12
F2A3	2.3	1.2

These findings are in agreement with Moyer (2007) who found the high resolution georeferenced ortho-mosaics very useful for conservation planning, vegetation and threat assessment but stated that the system does not perform well with automatic settings and requires a relatively large amount of time for manual image processing, especially in areas with extreme topographic relief.

In our case, ground control points were generated using the official orthorectified imagery for common features with the UAV images which is a practical and low cost approach. In other studies the geometrical accuracy of the mosaics was reported to be between one and two pixels when ground control points (measured with precision GPS) have been used in mosaic processing and between three and eight pixels without ground control points depending on terrain and light conditions (Ayebare et al. 2011)

An important limitation of ENSOMOSAIC is that it requires a fine calibration of camera optics, which has to be performed with additional commercial software, increasing the operational cost. This is especially important when different sensors are being investigated which is common in research studies.

4.4 Conclusion

Processing imagery to create georeferenced orthorectified mosaics is possible using ENSOMOSAIC for an area with strong relief but it required more time than expected, and the time used for learning how to use the different settings and adjust them for each flight condition should be considered also.

A lot of attention should be paid during the first level of processing which affects the quality of the whole mosaic in all stages and in order to avoid mistakes that could significantly increase the processing time.

The geometrical errors found in mosaics 1 and 2 were not acceptable for most applications and therefore planning should include an overlap exceeding the minimum overlap requirements by the software.

Insufficient overlap (forward<50% and side<40%) between images and having a single flight line result on mosaics with severe geometric errors (mean 22.8 m) despite intensive effort on refining all interactive settings within ENSOMOSAIC. In contrast, when the overlap was increased as on *Pla de la Calma* site, the resulting mosaic is of much higher quality (mean 2.3m).

4.5 References

3axis Image. 2012. Accessed October 13. http://quest.arc.nasa.gov/aero/virtual/demo/aeronautics/tutorial/images/3axis.gif.

Ayebare, S., D. Moyer, A. J. Plumptre, and Y. Wang. 2011. "Remote Sensing for Biodiversity Conservation of the Albertine Rift in Eastern Africa." http://www.ltrs.uri.edu/personal/K11949_C010.pdf.

"EnsoMOSAIC Image Processing User's guide v.7.3." 2009. MosaicMill.

Lobo Aleu, Agustín. 2009. "Testing low-altitude infrared digital photography from a mini-UAV to retrieve information for biological conservation". Info:eu-repo/semantics/report. http://www.recercat.cat/handle/2072/40714.

Marti Boada, Sonia Sanchez, Josep Pujantell, and Diego Varga. 2010. "Indicadores de cambio global en la Reserva de la Biosfera del Montseny, España." In *Reservas de la biosfera: su contribución a la provisión de servicios de los ecosistemas; experiencias exitosas en Iberoamerica*, 161–178. France. unesdoc.unesco.org/images/0018/001877/187732s.pdf.

Moyer, D. 2007. *Aerial Digital Mapping of the Eastern Arc Mountains and Coastal Forests of Tanzania and Kenya*. FINAL PROJECT COMPLETION REPORT. Wildlife Conservation Society. http://www.cepf.net/Documents/Final_WCS_AerialMonitoringTanzania.pdf.

Pellikka, Petri K.E., Milla Lötjönen, Mika Siljander, and Luc Lens. 2009. "Airborne Remote Sensing of Spatiotemporal Change (1955–2004) in Indigenous and Exotic Forest Cover in the Taita Hills, Kenya." *International Journal of Applied Earth Observation and Geoinformation* 11 (4) (August): 221–232. doi:10.1016/j.jag.2009.02.002.

Swain, Kishore C., Hemantha P. Jayasuriya, and Vilas M. Salokhe. 2007. "Suitability of Low-altitude Remote Sensing Images for Estimating Nitrogen Treatment Variations in Rice Cropping for Precision Agriculture Adoption." *Journal of Applied Remote Sensing* 1 (1): 013547. doi:10.1117/1.2824287.

5.1 General Conclusions

The use of unmanned aerial vehicles is increasing in multiple environmental and agricultural applications. They are especially useful for monitoring vegetation since these systems can acquire imagery with more spatial and temporal resolution than conventional systems (satellites and aircrafts) with a lower operational cost which permits the tracking of different plant stages and their changes towards climatic or anthropogenic influences.

However, in order to use imagery's information to its maximum potential, planning should account for processing requirements and usage of the new data, otherwise image processing could be costly and time consuming.

In chapter 1, it was proved that conventional color imagery acquired from a UAV is sufficient to produce maps of crop cover, allowing for the accurate location of areas of low crop vigor, and thus for taking the appropriate management decisions, at the specific sites. In other words, UAV imagery is cost-effective and valid as a basis for precision agriculture of sugar cane.

Nevertheless, two important aspects were also identified. First, multispectral imagery including the NIR part of the electromagnetic spectrum would greatly improve the resulting products as is well known from the experience gained from satellite and manned airborne imagery. Second, simple geometric correction methods that worked reasonably well in a flat area as the one of the sugarcane case study had to be evaluated on a larger area and more rugged terrain.

The geometric correction of imagery was addressed on the 2nd and 3rd chapter. The second chapter clearly indicated that standard empirical methods based on polynomial fitting are insufficient to cope with the particular distortions of these images. Instead, methods based on bundle block adjustment technology and automatic detection of tie points between images as those used in the third chapter, revealed to be able to produce orthorectified mosaics with a

reasonable error, albeit with a considerable (and more than expected) investment of human time. In addition, recording the flight angles was identified as opportunity to speed up processing and accuracy of the products.

Comparing these platforms with traditional ones, they offer four major advantages: they are considered more cost- effective, they minimize the risk to a pilot's life and provide more spatial and temporal resolution than satellite and aircraft based systems. These characteristics make them suitable for linking ground-based observations and remotely sensed imagery from aerial and satellite platforms.

Some limitations are coverage, sensors availability and strong winds. The flight autonomy is based on energy consumption and flight varies extensively depending of the UAV used from minutes to weeks but covering less area than satellites or traditional aircrafts. For instance, cropcam UAV used in chapter one can cover up to 100 ha with ~0.10 m resolution while satellites like SPOT have a footprint of 3600 sq. km with 2.5 m. Since the technology is relatively new for civil applications, there are less sensor availability on the market which have to be adjusted or created to meet space, weight and energy UAV capabilities. However, many efforts and research are being carried out developing new sensors and the availability of UAV operated sensors is increasing rapidly. Comparing the UAVs and piloted aircrafts with satellites, they offer sensor flexibility which is essential for research in which many sensors can be easily changed, not possible using satellites.

Comparing the prices and time restrictions, satellites and aircraft requires a minimum of several hundreds dollar for booking a satellite or renting a aircraft which in the case of weather restrictions can rise the price of monitoring drastically. As a example one SPOT image (2.5 m resolution) cost a minimum of 1200 dollars without full processing that could cost more. In contrast UAV services in Nicaragua cost ~400 dollars for each flight. In that sense, if the area to monitored is large, satellites are the best option regarding the price. But if time of acquisition, spatial resolution and area is small, then UAV are a suitable

options.

UAV can fly under clouds and at lower altitudes but not under strong wind conditions, which reflects the compatibility with other remote sensing platforms. It has be noticed that there is not a general solution for every need, and sometimes a combination of several tools can give the best results.

The general conclusion of this thesis is that imagery acquired with UAV is a cost-effective solution for environmental and agricultural applications of remote sensing. Nevertheless, it requires substantial effort and know-how on image processing.

5.2 References

Arjomandi, M. 2007. “Classification of Unmanned Aerial Vehicles.” *The University of Adelaide, Australia*. http://personal.mecheng.adelaide.edu.au/maziar.arjomandi/aeronautical%20engineering%20projects/2006/group9.pdf.

Biesemans, J., and J. Everaerts. 2006. “Image Processing Workflow for the PEGASUS HALE UAV Payload.” In *2nd International Workshop “‘The Future of Remote Sensing.’”(ISPRS Inter-Commission Working Group I/V Autonomous Navigation). Available Online at: Http://www. Pegasus4europe. Com/pegasus/workshop/proceedings/htm (accessed 11 June 2008)*. http://medusa.vgt.vito.be/modules/publications/documents/Biesemans_FRS_ANtwerp_2007.pdf.

Burdekin, D., P. Csóka, J. Kämäri, P. Kauppi, G. Landmann, S. Miina, R. Päivinen, A. Schuck, and H. Sterba. 2002. *External Review of the Finnish Forest Condition Monitoring Programme*. European Forest Institute. http://www2.euflegt.efi.int.qa.ambientia.fi/files/attachments/publications/ir_12.pdf.

Cramer, Wolfgang, Alberte Bondeau, F. Ian Woodward, I. Colin Prentice, Richard A. Betts, Victor Brovkin, Peter M. Cox, et al. 2001. “Global Response of Terrestrial Ecosystem Structure and Function to CO2 and Climate Change: Results from Six Dynamic Global Vegetation Models.” *Global Change Biology* 7 (4): 357–373. doi:10.1046/j.1365-2486.2001.00383.x.

Dunford, R., K. Michel, M. Gagnage, H. Piégay, and M.-L. Trémelo. 2009. “Potential and Constraints of Unmanned Aerial Vehicle Technology for the Characterization of Mediterranean Riparian Forest.” *International Journal of Remote Sensing* 30 (19): 4915–4935. doi:10.1080/01431160903023025.

Grenzdörffer, G. J., A. Engel, and B. Teichert. 2008. “The Photogrammetric Potential of Low-cost UAVs in Forestry and Agriculture.” *The International Archives of the Photogrammetry, Remote Sensing and Spatial Information Sciences* 31 (B3): 1207–1214.

Guo, T., Kujirai, T., and Watanabe, T. 2012. “MAPPING CROP STATUS FROM AN UNMANNED AERIAL VEHICLE FOR PRECISION AGRICULTURE APPLICATIONS.” In Vol. Volume XXXIX-B1, 2012. Melbourne, Australia: International Archives of the Photogrammetry, Remote Sensing and Spatial Information Sciences.

Hugh Turral, Jacob Burke, and Jean-Marc Faurès. 2011. *Climate Change, Water and Food Security*. FAO Water Report. Rome: Food and Agriculture Organization of the United Nations (FAO). http://www.google.es/url?sa=t&rct=j&q=agriculture%20is%20a%20key%20part%20of%20the%20puzzle%20of%20understanding%20climate%20change%20and%20the%20main%20source%20of%20food%20for%20mankind.&source=web&cd=1&cad=rja&ved=0CCEQFjAA&url=http%3A%2F%2Fwww.fao.org%2Fdocrep%2F014%2Fi2096e%2Fi2096e.pdf&ei=sT6JUPWaGtKIhQfkxYGoCg&usg=AFQjCNHRup_bFT-XUqNK5z_z6dUHMkvFPQ.

Johnson, E. N., and D. P. Schrage. 2004. “System Integration and Operation of a Research Unmanned Aerial Vehicle.” *System*. http://smartech.gatech.edu/handle/1853/36909.

Khan, Amir, David Schaefer, Lei Tao, David J. Miller, Kang Sun, Mark A. Zondlo, William A. Harrison, Bryan Roscoe, and David J. Lary. 2012. “Low Power Greenhouse Gas Sensors for Unmanned Aerial Vehicles.” *Remote Sensing* 4 (5) (May 9): 1355–1368. doi:10.3390/rs4051355.

Laliberte, Andrea S., Mark A. Goforth, Caitriana M. Steele, and Albert Rango. 2011. “Multispectral Remote Sensing from Unmanned Aircraft: Image Processing Workflows and Applications for Rangeland Environments.” *Remote Sensing* 3 (11) (November 21): 2529–2551. doi:10.3390/rs3112529.

Lobo Aleu, Agustín. 2009. “Testing low-altitude infrared digital photography from a mini-UAV to retrieve information for biological conservation”. Info:eu-repo/semantics/report. http://www.recercat.cat/handle/2072/40714.

Morris, Jefferson. 2003. “Northrop Grumman Modifies BQM-34 Firebee To Drop Payloads.” *Aerospace Daily*, January 22.

Niethammer, U., Rothmund, S., Schwaderer, U., Zeman, J., and Joswig, M. 2011. “OPEN SOURCE IMAGE-PROCESSING TOOLS FOR LOW-COST UAV-BASED LANDSLIDE INVESTIGATIONS.” In *International Archives of the Photogrammetry, Remote Sensing and Spatial Information Sciences*, Vol. XXXVIII-1/C22:2011. Zurich, Switzerland.

Thiele, A., E. Cadario, K. Schulz, U. Thoennessen, and U. Soergel. 2008. “Building Reconstruction from InSAR Data by Detail Analysis of Phase Profiles.” In *Proceeding of XXI Congress of ISPRS, China*. http://www.ipi.uni-hannover.de/uploads/tx_tkpublikationen/Thiele_Peking_08.pdf.

Towler, Jerry, Bryan Krawiec, and Kevin Kochersberger. 2012. “Terrain and Radiation Mapping in Post-Disaster Environments Using an Autonomous Helicopter.” *Remote Sensing* 4 (7) (July 5): 1995–2015. doi:10.3390/rs4071995.

Appendix

Example of Input Files

Calma.trp

```
# Updated Mon Oct 29 22:50:10 2012
Projection: NUTM 3 WGS84 WGS84ED50
Calibration_file: C:\ENSO\Camera\Sigma_DP1.cal
Ground_control_point_file: C:\ENSO\Areas\MONTSENY_PLACALMA\enso\placalma.gcp
Approximate_terrain_altitude: 1226.3
Camera_rotation: 270
Map_files: 0
# flight line,frame,image,directory
1   3 SDIM1440_tiled.tif C:\ENSO\Areas\MONTSENY_PLACALMA\TIFFOri\
1   4 SDIM1441_tiled.tif
1   5 SDIM1442_tiled.tif
1   6 SDIM1443_tiled.tif
1   7 SDIM1444_tiled.tif
```

Calma.gps

```
#flight line,frame,X,Y,altitude, bearing (degrees) ,day, time, year
1 3 2.330522074        41.7644252459 1913   21.6   Sep 26 10:09:15      2009
1 4 2.3343648188 41.7650960696      1881   121.3  Sep 26 10:09:56      2009
1 5 2.3378375096 41.7643235316      1855   90.8   Sep 26 10:10:17      2009
1 6 2.3415305148 41.763173862       1841   117.5  Sep 26 10:10:38      2009
1 7 2.3450276263 41.7623472047      1823   104.5  Sep 26 10:10:58      2009
```

Calma.cal

```
% Calculation: CalCam PRO version 1.1.1
Camera          Sigma/DP1/1025922
Lens            IRF
Owner           CSIC, Catalunia
Number_of_channels 1
Channel_id                              1
Focal_length      2146.662844226738300000000000
Principal_point_x 1324.742154856953000000000000
Principal_point_y  877.792275920020070000000000
General_scaling      0.001000000000000000000000
Affinity            2.010155700894416000000000
Radial_k1          -16.207181350255709000000000
Radial_k2            3.433290131227360000000000
Radial_k3           -0.129823625049993450000000
Tangential_t1       -0.250790099255155770000000
Tangential_t2        0.176585653618481080000000
Un-orthogonality     0.296005645665524730000000
Sensor_width                    2640   20.7000
Sensor_height                   1760   13.8000
```

Calma.gcp

```
#point,X,Y,Z,weights for x,y and z

1 445226.20  4623884.00 1287.68 0.3 0.3 0.8
2 443672.20  4623076.00 1159.17 0.3 0.3 0.8
3 442980.80  4622800.00 1120.19 0.3 0.3 0.8
4 442155.90  4622793.00 1036.25 0.3 0.3 0.8
5 441630.90  4621921.00  958.66 0.3 0.3 0.8
6 442760.80  4622091.00  980.03 0.3 0.3 0.8
7 444493.10  4623615.00 1236.62 0.3 0.3 0.8
8 445981.70  4623828.00 1294.74 0.3 0.3 0.8
```